PharmaNutrition 37 (2026) 100527

Contents lists available at ScienceDirect

PharmaNutrition

journal homepage: www.elsevier.com/locate/phanu

Fermented *Musa paradisica* fruit pulp extract attenuates dyslipidemia, and pancreatic, jejunal and neuronal dysfunctions in streptozotocin-induced diabetes in rats

Adeleke Kazeem Atunnise [a,*], Paul Gbenga Awoniran [b], Olusegun Lateef Adebayo [a], Adewale Adewuyi [c], Bamidele Adewale Salau [a]

[a] Department of Biochemistry, Faculty of Basic Medical Sciences, Redeemer's University, Ede, Osun State, Nigeria
[b] Department of Human Anatomy, Faculty of Basic Medical Sciences, Redeemer's University, Ede, Osun State, Nigeria
[c] Department of Chemical Sciences, Faculty of Natural Sciences, Redeemer's University, Ede, Osun State, Nigeria

ARTICLE INFO

Keywords:
Fermentation
Diabetes mellitus
Intestinal function
Antioxidant
Anti-inflammation

ABSTRACT

Persistent hyperglycemia is the hallmark of diabetes mellitus, and it involves complex metabolic and neuro-enteric disturbances that challenge single-target therapies. Fermentation of *Musa paradisiaca* (plantain) fruit pulp has previously been reported as a means of enhancing its bioactivity, which may exert multifaceted nutraceutical benefits, including metabolic regulation. We tested the hypothesis that fermented *M. paradisiaca* fruit pulp methanolic extract (*f*-PUME) normalises body weight and fasting glycaemia, attenuates dyslipidaemia, preserves pancreatic β-cell mass and function via antioxidant and anti-inflammatory actions, and maintains the integrity of hypothalamic and jejunal morphology. Thirty adult male Sprague–Dawley rats were randomised into five groups: control, STZ-only, STZ + glibenclamide (5 mg/kg), STZ + unfermented extract (100 mg/kg), and STZ + fermented extract (100 mg/kg). Hyperglycemia was induced with a single i.p. STZ injection, followed by 42 days of daily oral treatment. Body weight, glucose regulatory, coronary, and atherogenic indices, oxidative stress biomarkers, pancreatic proinflammatory cytokines, brain, jejunal, and pancreatic organosomatic indices, and their histomorphometry were assessed. By Day 14, *f*-PUME reversed STZ-induced weight loss and fasting hyperglycaemia. *f*-PUME modestly lowered total cholesterol and triglycerides while preserving HDL-c, normalising Castelli and atherogenic indices. In the pancreas, *f*-PUME restored organ weight, boosted insulin secretion, reactivated antioxidant enzyme activities, and suppressed MDA and proinflammatory cytokine levels, thereby preserving islet architecture and β-cell granule density. *f*-PUME also reversed hypothalamic- and jejunal-vacuolation and pyknotic nuclei and repaired jejunal crypt morphology. *f*-PUME exhibits a marked anti-hyperglycemic effect via antioxidant, glucose and lipid metabolic normalisation, organoprotection, and entero-neuronal morphological and functional restoration.

1. Introduction

Persistent hyperglycemia is synonymous with diabetes mellitus (DM) [1]. The combination of type I and type II has consistently maintained the top spot in global health crisis indices. DM affects an estimated 588.7 million people worldwide in 2024 [2]. It is projected to increase by 45% by 2050 [2,3]. DM is a multifactorial metabolic disorder characterised by chronic hyperglycemia and progressive β-cell dysfunction, which collectively precipitate a cascade of systemic complications encompassing cardiovascular disease, nephropathy, neuropathy, and enteropathy [1,2]. At the cellular level, sustained elevations in circulating glucose lead to an excessive generation of reactive oxygen species (ROS) through enhanced mitochondrial electron transport chain leakage, increased flux in the polyol pathway, and non-enzymatic protein glycation [4]. The resultant oxidative milieu overwhelms intrinsic antioxidant defences such as superoxide dismutase (SOD), catalase (CAT), and glutathione peroxidase (GPx), culminating in lipid peroxidation, protein carbonylation, DNA strand breaks and activation of nuclear factor-κB (N*F*-κB)-mediated proinflammatory cascades within pancreatic islets [5,6].

* Corresponding author.
E-mail addresses: adelekeatunnise@gmail.com, atunnisea@run.edu.ng (A.K. Atunnise).

https://doi.org/10.1016/j.phanu.2026.100527
Received 30 October 2025; Received in revised form 28 April 2026; Accepted 7 August 2026
Available online 9 August 2026
2213-4344/© 2026 Elsevier B.V. All rights are reserved, including those for text and data mining, AI training, and similar technologies.

Moreover, hyperglycemia-induced dyslipidemia is characterised by elevated low-density lipoprotein cholesterol (LDL-c) and triglycerides (TG), and reduced high-density lipoprotein cholesterol (HDL-c). Thus, DM serves as a potent driver of atherosclerotic plaque formation and vascular thrombosis [7,8]. This lipoprotein imbalance exacerbates not only endothelial dysfunction through oxidative modification of apolipoproteins but also perpetuates inflammatory signalling in vascular smooth muscle and macrophages, thereby amplifying cardiovascular risk [4,7,8].

Beyond these classical paradigms, emerging evidence implicates the neuro-enteric channel as a critical contributor to DM pathogenesis and its attendant neurological and enteric sequelae [6]. Also, DM is considered an independent risk factor of ischemic stroke, and coupled with the fact that some specific classes of antidiabetes drugs may even exhibit prooxidant effects, potentially exacerbating neurodegenerative processes [9,10]. Within the enteric region, hyperglycemia has been reported to induce disrupted intestinal barrier integrity. This condition facilitates the translocation of microbial lipopolysaccharide (m-LPS) into the circulatory system, thereby promoting systemic endotoxemia and microglial activation in hypothalamic and hippocampal nuclei [11,12]. This neuroinflammatory process disrupts central regulation of energy homeostasis, insulin sensitivity, and neurotransmitter synthesis, thereby further perturbing glycemic control [13–15]. Additionally, oxidative stress within the central nervous system has been reported to impair Na^+/K^+-ATPase function and cholinergic neurotransmission. This mechanism has been intimately linked to diabetic-induced cognitive impairment and autonomic neuropathy [16–19].

To date, conventional antidiabetic medications such as biguanides, sulfonylureas, thiazolidinediones, dipeptidyl peptidase−4 inhibitors (DPP4-i), and sodium-glucose co-transporter 2 inhibitors (SGLT2-i) have achieved significant success in glycemic normalisation. However, they often fall short of rectifying other diabetic complications, primarily oxidative and inflammatory derangements, or of restoring enteroneuronal functions and integrity [20,21]. Indeed, evidence suggests that some of these medications may inadvertently generate prooxidant metabolites; hence, limiting their therapeutic benefits [9,10]. In this context, natural product-based interventions, especially nutraceuticals, have attracted considerable interest due to their multitargeted bioactivities.

Musa paradisiaca (plantain), a rich source of phenolic acids, flavonoids, resistant starch, and oligosaccharides, is known to possess antioxidant, anti-inflammatory, and prebiotic properties [22–24]. Fermentation of *M. paradisiaca* fruit pulp by endogenous or probiotic microbiota significantly enhances the liberation and bioavailability of these bioactives. Hence, the phytoconstituents of fermented *M. paradisiaca* fruit pulp have been documented to enhance free-radical scavenging capacity, attenuate NF-κB signalling, and modulate microbial ecology [22,25]. Toxicological evaluations in rodent models further confirm that fermented *M. paradisiaca* preparations are safe at therapeutic doses and can improve lipid profiles and atherogenic indices, underscoring their translational potential [26,27].

Against the multifaceted pathophysiological indices, the present study was set to investigate the hypothesis that fermented *M. paradisiaca* fruit pulp methanolic extract (*f*-PUME) exerts a protective effect on the pancreas, brain and jejunal regions, in addition to metabolic modulation in STZ-induced hyperglycemic in male rats. Hence, this study seeks to establish *f*-PUME as a multitargeted candidate for the management of hyperglycemia in diabetic conditions.

2. Materials and methods

2.1. Animal management and treatment

A total of thirty adult male Sprague-Dawley rats (average weight: 150 ± 10 g) were obtained from the Department of Physiology, Faculty of Basic Medical Sciences, University of Ibadan, Oyo State, Nigeria. Upon arrival, animals were individually housed in ventilated polypropylene cages lined with autoclaved wood shavings as bedding. The animal housing environment was maintained at 25 ± 1°C and 55 ± 5% relative humidity. Also, the rats were kept under a natural photoperiod with a 12-hour light/dark daily cycle. These conditions were implemented to reduce environmental stress and ensure animal welfare throughout the study. Animals were allowed a two-week acclimatisation period prior to experimental interventions. During this period, all rats had unrestricted access to commercial rodent chow (Ladokun Feeds, Ibadan, Nigeria) and clean tap water. Food and water were replenished daily, and cage hygiene was routinely maintained to limit microbial exposure. All animal procedures were performed in accordance with internationally accepted ethical principles and regulatory standards. The study protocol was reviewed and approved by the Redeemer's University Institutional Animal Care and Use Committee (RUN-IACUC), with ethical approval number RUN/REC/2025/327. Animal handling and experimental procedures complied with the Guide for the Care and Use of Laboratory Animals (8th Edition, National Research Council, 2011) and adhered strictly to the ARRIVE guidelines to ensure methodological transparency, reproducibility, and humane care of animals.

2.2. Experimental design and grouping

After a two-week acclimatisation period, thirty adult male Sprague-Dawley rats (average body weight: 150 ± 10 g) were randomly divided into five experimental groups (n = 6 per group) using stratified randomisation based on body weight. The experimental groups and their treatments were as follows:

Control Group (CG): Received a single intraperitoneal injection of vehicle (0.05 M citrate buffer, pH 4.5) and no further treatment throughout the study duration.

STZ-Only Group (SO): Induced with diabetes via a single intraperitoneal injection of streptozotocin (STZ) at a dose of 65 mg/kg body weight, prepared in 0.05 M citrate buffer (pH 4.5), without further treatment.

STZ + Glibenclamide (a known drug) Group (SD): Diabetes induced with STZ as above and treated orally with glibenclamide (5 mg/kg body weight [28]) once daily.

STZ + Unfermented *M. paradisiaca* Fruit Pulp Extract Group (SU): Diabetes induced with STZ and treated orally with unfermented *M. paradisiaca* pulp methanolic extract at a dose of 100 mg/kg body weight once daily (50% of the dose reported in *M. paradisiaca* pulp extract [29].

STZ + Fermented *M. paradisiaca* Fruit Pulp Extract Group (SF): Diabetes induced with STZ and treated orally with fermented *M. paradisiaca* pulp methanolic extract at a dose of 100 mg/kg body weight once daily.

All treatments were administered by oral gavage from the time of diabetes confirmation. The intervention was introduced to the diabetic rats and continued daily for 42 consecutive days. The treatment schedule was standardised across all groups to control for circadian influence on metabolic parameters.

2.2.1. Induction of diabetes

On experimental Day 1, all animals in (SO, SD, SU, and SF) were fasted for 6–8 h prior to the induction of diabetes, whereas the control group (CG) was maintained under normal feeding conditions. A 0.05 M sodium citrate buffer (pH 4.5) was freshly prepared and used as the vehicle for streptozotocin (STZ). STZ (AK Scientific, Inc., USA; Catalogue No: E301) was dissolved in the citrate buffer to a final concentration of 10 mg/mL. It was prepared immediately before use to preserve its stability and potency. Each rat in the diabetic group received a single intraperitoneal (i.p.) injection of STZ at a dose of 65 mg/kg body weight using a sterile 1-mL syringe fitted with a 23-gauge needle, 15 min after initial i.p. administration of 230 mg/kg body weight nicotinamide [30]. Control rats (CG) were administered an equivalent volume of the sodium

citrate buffer via the same route. Following the injection, all animals were returned to their respective cages and provided with standard rat chow. To all the STZ groups, a 10% sucrose solution was given in place of regular drinking water to mitigate acute hypoglycemia typically observed after STZ administration [31]. On experimental day 2, the 10% sucrose solution was withdrawn and replaced with normal drinking water. Throughout the post-induction period, the rats were monitored for clinical signs of diabetes and behavioural changes, with body weights and general health recorded at regular intervals.

2.2.2. Confirmation of hyperglycemia

On the experimental day 3, all rats were fasted for 6–8 h. Blood glucose levels were measured from tail vein samples using a One Touch Basic Blood Glucose Monitoring System. Hyperglycemia was defined as a blood glucose level $>$ 150 mg/dL and/or statistically higher than that of control rats. Rats exhibiting hyperglycemia were considered validated diabetic models and included in the study [2,31,32].

2.2.3. Preparation and administration of plant extracts

The methanol extracts of both fermented and unfermented *M. paradisiaca* fruit pulp were prepared, as reported in our previous study [22]. Briefly, the *M. paradisiaca* fruit was thoroughly rinsed with clean water under a running tap in the Biochemistry laboratory unit of the Centre for Chemical and Biochemical Research building, Redeemer's University. The water on the fruit skin was allowed to drip completely, then the peel was removed and discarded. The peeled fruit was mechanically ground into its finest paste with sterile water (1:1 w/v) and inoculated for 15 min (spontaneous fermentation initiation) in a fermenting jar. The jar was placed in the sterile anaerobic, isothermal batch-fermenter (locally fabricated). The fermentation condition was set as 30 $\pm$ 1 ^{o}C temperature, 5% CO_2 evolution rate (CER), 150 rpm agitation and 1 bar pressure. After the 9th day, the fermented sample was mixed with absolute methanol (1:2, w/v) and agitated at 150 rpm for 30 min. This allows maximum dissolution and fermentation termination before filtering through a Whatman No. 1 filter paper. The filtrate was concentrated in a rotatory evaporator at 45 ^{o}C. The fermented *M paradisiaca* fruit pulp methanolic-extract (*f*-PUME) and unfermented *M paradisiaca* fruit pulp methanolic-extract (*u*-PUME) concentrates were prepared at a dose of 100 mg/kg body weight [33], using distilled water as the vehicle. The extracts were administered orally via gavage for 42 days. Glibenclamide (5 mg/kg body weight) was administered via the same route.

2.2.4. Sample collection and processing

At the end of the 42-day treatment period, the rats were fasted and weighed. The rats were euthanised (locally constructed CO_2 euthanasia chamber), and blood was collected from the heart using a syringe and placed in labelled EDTA tubes. The plasma was separated by centrifugation at 4000 rpm for 10 min at 4°C and stored at −20°C until further analysis. The pancreas, brain, and jejunum were carefully excised and cleared of extraneous fat and connective tissue. The tissues were rinsed in ice-cold 1.15% KCl and weighed. The tissue (pancreas, brain and jejunum) was homogenised in 0.1 M, pH 7.4 sodium phosphate buffer (1:10 w/v). The homogenate of each tissue was centrifuged at 5000 rpm (4 ^{o}C) for 10 mins. The supernatant collected was stored at −20 ^{o}C until required for analyses. Also, tissues from a representative rat in each group were fixed in a 10% formalin solution for histological analysis.

2.3. Organosomatic indices and protein concentrations

2.3.1. Organosomatic indices (OSI)

OSI were calculated by expressing the weight of each organ as a percentage of the final body weight of the rat, serving as a quantitative measure of relative organ hypertrophy or atrophy [34].

2.3.2. Total protein

Total protein concentrations in the brain, pancreas, jejunum, and plasma were estimated using the classical Lowry assay, which remains a gold standard for protein quantification due to its sensitivity and consistency. Protein concentrations were determined spectrophotometrically, using bovine serum albumin (BSA) as the reference standard [35]. Briefly, tissue homogenates or BSA standards (0–100 μg/mL) were added to alkaline copper reagent. The mixture was incubated for 10 min at room temperature, and Folin–Ciocalteu phenol reagent (diluted 1:1 with distilled water), vortexed, and incubated in the dark for 30 min. The chromophore was read spectrophotometrically at 750 nm, and protein concentration was calculated from a standard calibration curve and expressed as mg protein/mL of homogenate or mg/g tissue.

2.4. Plasma lipid profiling

Plasma triglycerides (TG), total cholesterol (TChol), and high-density lipoprotein cholesterol (HDL-c) levels were assayed using diagnostic kits from Randox Laboratories (UK) in accordance with the manufacturer's protocol [CAT NOs: HDL-c - CH3811, TG - TR3823, TChol - CH3810]. The level of low-density lipoprotein cholesterol (LDL-c) was indirectly calculated using the Friedewald equation: [36]

LDL (mg/dL) = TChol – HDL – (TG / 5) (applicable when TG $<$ 400 mg/dL).

To assess dyslipidemia-related cardiovascular risk, the following atherogenic and coronary heart disease indices were computed:

Non-HDLc = TChol – HDL-c

Castelli Risk Index I (CRI-I) = TChol / HDL-c

Castelli Risk Index II (CRI-II) = LDL / HDL-c

Atherogenic Index of Plasma (AIP) = log (TG / HDL-c)

Atherogenic Coefficient (AC) = (TChol – HDL) / HDL-c

These ratios are established surrogate biomarkers for evaluating atherogenic potential, particularly under diabetic and metabolic stress conditions [37–40].

2.5. Determination of oxidative stress biomarkers, brain acetylcholinesterase and Na^{+}/K^{+} ATPase activities

To assess oxidative stress and antioxidant defence status, specific biochemical markers were quantified in plasma and tissue homogenates (pancreas, brain, and jejunum) using validated spectrophotometric methods. All procedures were carried out at room temperature unless otherwise stated, and absorbances were measured using a UV–visible spectrophotometer (Jenway 6305).

2.5.1. Reduced glutathione (GSH)

GSH levels were measured using the method of Beutler et al. [41]. Briefly, 0.2 mL of tissue homogenate or plasma was mixed with 1.8 mL of 1.3% (w/v) sulfosalicylic acid and allowed to stand for 10 min at 4°C. The mixture was centrifuged at 2500 $\times$ g for 15 min. Then, 1 mL of the resulting supernatant was added to 4 mL of 0.1 M phosphate buffer (pH 7.4), followed by 0.5 mL of Ellman's reagent (5,5′-dithiobis-(2-nitrobenzoic acid); 0.01 M in methanol). The absorbance was read at 412 nm. GSH concentrations were extrapolated from a standard curve of reduced glutathione.

2.5.2. Nitric oxide (NO)

NO levels were determined using the Griess reagent method, as described by Bryan et al. [42]. Briefly, 0.5 mL of plasma or deproteinised tissue homogenate was mixed with 0.5 mL of Griess reagent, consisting of 1% sulfanilamide in 5% phosphoric acid and 0.1% N-(1-naphthyl)

ethylenediamine dihydrochloride. The mixture was incubated at room temperature for 10 min, and absorbance was measured at 540 nm. Nitrite concentrations were determined using sodium nitrite ($NaNO_2$) as a standard.

2.5.3. Malondialdehyde (MDA)

MDA levels, a marker of lipid peroxidation, were determined using the thiobarbituric acid reactive substances (TBARS) method described by Varshney et al. [43]. A 0.5 mL sample of tissue homogenate or plasma was mixed with 1.5 mL of 1% (w/v) phosphoric acid and 0.5 mL of 0.6% (w/v) thiobarbituric acid. The mixture was heated in a boiling water bath (95°C) for 45 min, then cooled and centrifuged at 3000 × g for 10 min. The supernatant absorbance was measured at 532 nm. MDA concentration was calculated using an extinction coefficient of $1.56 \times 10^5\ M^{-1}cm^{-1}$.

2.5.4. Catalase (CAT) activity

CAT activity was assayed following the method by Luck [44]. The decomposition of hydrogen peroxide (H_2O_2) was monitored by adding 0.1 mL of tissue homogenate to 2.9 mL of 30 mM H_2O_2 prepared in 50 mM phosphate buffer (pH 7.0). The decrease in absorbance was recorded at 240 nm over 1 min. One unit of CAT activity was defined as the amount of enzyme that decomposes 1 μmol of H_2O_2 per minute.

2.5.5. Glutathione S-transferase (GST) activity

GST activity was measured using the method of Nadarajapillai et al. [45]. The assay mixture contained 0.5 mL of 0.1 M phosphate buffer (pH 6.5), 0.1 mL of 1 mM reduced glutathione (GSH), 0.1 mL of 1 mM 1-chloro−2,4-dinitrobenzene (CDNB), and 0.3 mL of tissue homogenate or plasma. The increase in absorbance at 340 nm was measured for 5 min. Enzyme activity was calculated using the extinction coefficient of $9.6\ mM^{-1}cm^{-1}$ for the CDNB–GSH conjugate.

2.5.6. Superoxide dismutase (SOD) activity

SOD activity was assayed by the method of Misra et al. [46]. A 0.5 mL sample of tissue homogenate was added to 2.5 mL of 0.05 M carbonate buffer (pH 10.2). The reaction was initiated by adding 0.3 mL of freshly prepared 0.3 mM adrenaline (epinephrine) solution. The increase in absorbance was recorded at 480 nm every 30 s for 2 min. One unit of SOD activity was defined as the amount of enzyme required to inhibit the auto-oxidation of epinephrine by 50%.

2.5.7. Acetylcholinesterase (AchE) activity

Acetylcholinesterase activity was determined according to the method of Ellman *et al.* [47]. A 0.4 mL aliquot of tissue homogenate was added to a cuvette containing 2.6 mL of 0.1 M phosphate buffer (pH 8.0). DTNB reagent (0.1 mL) was then added. After 10 mins of incubation at 37 °C, the enzymatic reaction was initiated by the addition of 2.5 mM acetylcholine iodide (20 μL) [AKScientific, Inc., CAT NO: V1948], and the increase in absorbance at 412 nm was monitored for 3 mins. AChE activity was calculated from the linear change in absorbance per minute. As follows (ε = 13,600 M^{-1} cm^{-1}, path length = 1 cm, total reaction volume $=.12\times10^{-3}$ L): C_0*: initial tissue concentration (mg* mL^{-1}*),* 2: 2 moles of TNB^- formed per mole of acetylthiocholine hydrolyzed, V_{assay}: total reaction volume (L), *F*: dilution factor of aliquot (3.9), 10^{-3} conversion mg tissue to g tissue.

$$5.74 \quad X\,10^{-4} = \frac{2 \times V_{assay} \times F}{\varepsilon_{412} \times l \times 10^{-3}}$$

$$\textit{Rate of subtrate hydrolysis} \quad (\text{molmin}^{-1}\,g^{-1}\,\text{tissue}) = 5.74 \times 10^{-4}\ \frac{\Delta A \quad (412nm)}{C_{0(\text{mg mL}^{-1})}}$$

2.5.8. Na^+/K^+ ATPase activity

The Na^+/K^+-ATPase activity was estimated according to the Quigley & Gotterer [48] procedure. Na^+/K^+-ATPase activity was estimated as the difference between the total ATPase and Mg^{2+}-ATPase activities. Briefly, the ion-medium (7.5 mM Tris-HCl buffer, pH 7.2, 120 mM NaCl, 20 mM KCl, 7.5 mM MgSO4) was constituted to 400 μL (volume) for ATPase, ouabain-sensitive medium, and control assays, respectively. A 100 μL of tissue homogenate was added to ATPase and ouabain-sensitive media only. A 100 μL of ouabain was added to the ouabain-sensitive medium only. While 100 μL ATP solution (7 mM ATP) was added only to the total ATPase and ouabain-sensitive mixtures. The equivalent amount of water required to make up to 900 μL of reaction mixtures were added to each of the three reaction mixtures. To initiate the reactions, 100 μL of 7 mM disodium-ATP was added to the total ATPase and ouabain-sensitive mixtures only and incubated for 15 mins at 37 °C. The reaction was terminated by adding 1 mL of cold 10% TCA to each of the three tubes. While 100 μL of tissue homogenate was added to the control test tube, afterwards. The aggregate of 2 mL reaction mixtures in each of the three tubes was centrifuged for 10 min at 3000 rpm. One millilitre of the supernatant was taken and used to quantify hydrolysed ATP. Stewart [49] spectrophotometry protocol (660 nm) was adapted to quantify inorganic phosphate produced, and results were expressed as nanomoles Pi/minute/mg protein.

2.6. Determination of Insulin, Inflammatory Cytokines and NF-κB by ELISA

Concentrations of insulin, CAT No.: E-EL-R2466, proinflammatory cytokines, interleukin−1 beta (IL-1β) – CAT No: E-EL-R0012, interleukin−6 (IL-6) - CAT No.: E-EL-R0015, tumour necrosis factor-alpha (TN*F*-α) – CAT No.: E-EL-R2856, as well as the transcription factor nuclear factor kappa B (N*F*-κB) – CAT No.: E-CL-H0902, were quantified using enzyme-linked immunosorbent assay (ELISA) kits (Elabscience Biotechnology Inc., Houston, TX, USA). All assays were conducted at Brainwill Laboratory Limited, Osun State, Nigeria.

2.6.1. Immuno-quantification of pancreatic insulin level

The insulin assay was carried out according to the manufacturer's manual instructions. In brief, 100 μL of appropriately diluted homogenate samples or standards were added to the wells of pre-coated 96-well microplates. Plates were incubated at 37 °C for 90 min to allow antigen binding. The unbound mixture was discarded, and 100 μL of rat-specific biotinylated detection antibody was added and incubated for 1 h at 37 °C. Plates were aspirated, rewashed (3 cycles). Avidin-Horseradish Peroxidase-conjugated solution (100 μL) was added and incubated for 30 min at 37 °C. After an additional 5 washes, 90 μL of 3,3′,5,5′-tetramethylbenzidine (TMB) substrate solution was added to each well and incubated in the dark for 15 min. The reaction was stopped by adding 50 μL of stop solution, and the absorbance was read immediately at 450 nm using a microplate reader. Quantification was based on standard curves generated from known concentrations of recombinant protein supplied with the kits, and the detection is 6.25–400 pg/mL.

2.6.2. Immuno-quantification of pancreas cytokines and NF-κB

Cytokines and NF-κB assays were performed according to the manufacturer's standard protocols. Briefly, 100 μL of appropriately diluted homogenate samples or standards were added to the wells of pre-coated 96-well microplates. Plates were incubated at 37 °C for 90 min to allow antigen binding. After washing three times with wash buffer (300 μL/well), 100 μL of biotinylated detection antibody was added and incubated for 1 h at 37 °C. Plates were rewashed and incubated with 100 μL of horseradish peroxidase (HRP)-conjugated secondary antibody for 30 min at 37 °C. Following additional washing, 90 μL of TMB substrate solution was added to each well and incubated in the dark for 15 min. The reaction was stopped by adding 50 μL of stop solution, and the absorbance was read at 450 nm using a microplate reader. Quantification was based on standard curves generated from known concentrations of recombinant substrate supplied with the kits. The detection

ranges were as follows: INS (0.31–20 ng/mL), IL-1β (15.6–1000 pg/mL), IL-6 (31.25–2000 pg/mL), TN*F*-α (15.6–1000 pg/mL), and N*F*-κB (62.5–4000 pg/mL).

2.7. Histological processing and digital morphometric analysis

2.7.1. Histological processing

Pancreas, brain (hypothalamus), and jejunum tissues were fixed in 10% formalin for 24 h [50], processed through graded ethanol and xylene, and embedded in paraffin. Section (3 μm) were stained with hematoxylin and eosin (H&E) for general morphology and with Gomori aldehyde–fuchsin for pancreatic β-cell visualisation [51]. All slides were prepared at the Anatomy Laboratory, Obafemi Awolowo University, Ile-Ife, Nigeria. Digital images were captured using an Amscope DM500 camera. The pancreas was captured at x10 and x40, the hypothalamus (brain region) at x4 and x40, and the jejunum at x4 only, using the objective lenses.

2.7.2. Digital morphometric analysis

Quantitative morphometry and histologic scoring were performed in ImageJ v1.53c (NIH, USA) [52] on calibrated digital micrographs. All measurements were based on direct planimetric or linear geometry, with counts normalised to defined tissue areas. Pathology indices, including inflammatory cell infiltrates, necrotic debris, and vacuole counts, were scored using a 10 × 10 grid overlay and the multi-point tool. Analyses were conducted by an observer blinded to experimental groups. Pancreatic H&E-stained sections (×400), individual islets were manually delineated. Islet area ($\times 10^3$ μm^2) and perimeter ($\times 10^2$ μm) were obtained from traced boundaries. Nuclear profiles were counted within each islet and normalised to islet area to determine nuclear density (/10, 000 μm^2). Inflammatory cells, necrotic debris, and cytoplasmic vacuoles were identified by morphology and quantified within the same islet regions. These measurements follow established quantitative approaches for pancreatic islet morphometry, including normalisation of cellular counts to endocrine area [53].

For Gomori aldehyde fuchsin-stained pancreatic sections (×400), the number per field was recorded. Mean islet diameter was calculated as the average of orthogonal Feret diameters, and estimated islet area ($\times 10^3$ μm^2) was derived from planar measurements [54]. Aldehyde fuchsin–positive area was segmented using consistent colour-thresholding parameters and expressed as a percentage of total islet area. Vacuolation was quantified as the percentage of islet area lacking aldehyde fuchsin signal. Islet border integrity was assessed on a semi-quantitative 0–5 scale based on perimeter continuity. β-cell density was calculated as aldehyde fuchsin–positive nuclear counts normalised to endocrine area (×10 cells/10^4 μm^2), and islet size and β-cell density measurements align with established quantitative islet analyses [55,56].

In the hypothalamic (brain region) H&E-stained sections (×40), identical measurement rules were applied to defined regions of interest. Nuclear counts were normalised to region area to calculate nuclear density (/100 μm^2), and vacuoles were quantified using the same criteria; this was done using the ImageJ workflow. For jejunal H&E-stained sections (×40), villus height was measured from the villus tip to the villus-crypt junction, and crypt depth was measured from the crypt base to the same junction. Villus width was measured at mid-villus, total mucosal thickness from the muscularis mucosae to the villus tip, and villus density was calculated as villi per millimetre of mucosal length. The villus height-to-crypt depth (VH:CD) ratio was calculated from paired measurements within the same field [57].

2.8. Statistical analysis

All quantitative data are expressed as mean ± standard deviation (M ±SD) and n = 6. Prior to inferential testing, data sets were evaluated for normality using the Shapiro–Wilk test and for homogeneity of variances by Levene's test. Statistical analyses were performed in GraphPad Prism 9.0 (GraphPad Software, San Diego, CA, USA). Comparisons among treatment groups were made using one-way analysis of variance (ANOVA), and when the ANOVA reached significance, a post hoc test using Tukey's multiple comparisons was used to determine individual group differences. Data were considered statistically significant at $p < 0.05$.

3. Results

3.1. Effects of fermented M. paradisiaca pulp methanolic extract (f-PUME) on body weight and glycemic parameters in STZ-induced diabetes rats

The change in the body weight of rats was represented in Fig. 1A. At day 1, body weight change did not differ significantly among the control group (CG), STZ-only group (SO), STZ + glibenclamide (SD), STZ + unfermented extract (SU), and STZ + fermented extract (SF) ($p > 0.05$). By day 7, the CG body weight was significantly higher ($p < .0.05$) than the diabetes groups (SO, SD, SU and SF), and this increase was sustained till the end, except in the SF, which was not significantly different ($p > 0.05$) from days 14 to the end. SO and SD had no significant difference in body weight from day 1–42 ($p > 0.05$). Between SO and SF, a significant difference ($p < 0.05$) was noted at days 7 and 28–42. Within the diabetes groups, SD and SU showed a significant difference ($p < 0.05$) at days 7 and 35 only; SD was significantly different from SF at days 7, 35 and 42 only, and SU and SF were significantly different at day 28 only.

In Fig. 1B, the weekly fasting blood glucose (FBG) level in the diabetes group was significantly higher ($p < 0.0001$) than that of the CG from days 1–14. At days 21 and 28, SO, SD and SU FBG levels remained significantly higher ($p < 0.0001$) than CG; whereas SF value was not significantly different from CG ($p > 0.05$) from day 21 to the end of the experiment. The FBG levels in SU and SD were not significantly different from those in CG at days 35 and 42, respectively ($p > 0.05$). Among the treatment groups (SD, SU, and SF), FBG levels in SD and SU were not significantly different ($p > 0.05$) at days 7–42. SD and SF showed a significant difference ($p < 0.001$) only at days 21–35. Between the *M. paradisiaca* treatment groups (SU and SF), SU differed significantly ($p < 0.05$) from SF only at days 1 and 14–28.

During the oral glucose tolerance test (Fig. 1C), at baseline (0 min), CG blood glucose (BG) was significantly ($p < 0.0001$) lower than SO and SU only. Thirty minutes later, only SO, SU and SF BG were significantly ($p < 0.001$) different from CG. At 60 min, only SO and SU were not different from the CG ($p > 0.05$). At 120 mins, only SU was not significantly different ($P < 0.05$) from the CG. At 150 min, SO and SU were significantly ($p < 0.05$) higher than the CG level. In the diabetic group, the three treatment groups' FBG levels were significantly lower ($p < 0.00001$) from 0 to 150 mins compared with SO, except for SU, which was not significant at 30 and 60 min. Between the treatment groups,

3.2. Effect of fermented M. paradisiaca fruit pulp methanolic extract on plasma lipid profile and atherogenic indices of STZ-induced diabetes in rats

In Fig. 2A, the plasma total cholesterol (TChol) of CG was not significantly different from the diabetes groups ($p > 0.05$). Between the diabetes groups, SU and SF were significantly different ($p < 0.05$) from SO, but no significant difference ($p > 0.05$) was noted among the treatment groups. The plasma triglycerides (TG) level in the diabetes groups was not significantly different ($p > 0.05$) from the CG group. Plasma high-density lipoprotein (HDL-c) level in SO and SD was significantly ($p < 0.001$) lower and higher than that of the CG, respectively. Within the diabetes groups, SD, SU and SF were significantly higher than SO ($p < 0.001$). Among the treatment groups, HDL-c in SD was significantly ($p < 0.05$) higher than in SU and SF, but no significant difference ($p > 0.05$) was observed between SU and SF. The LDL-c and

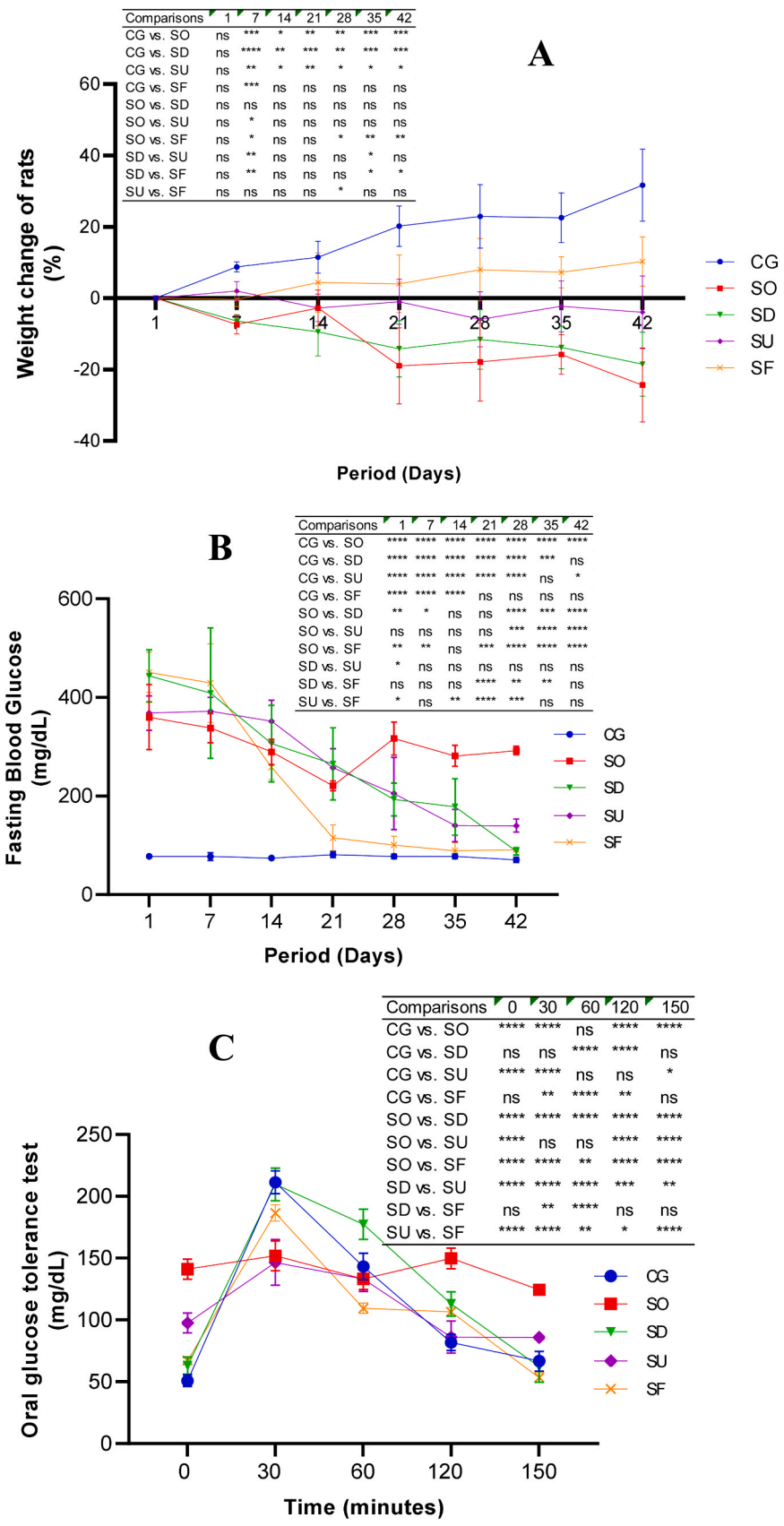


Fig. 1. Effect of fermented M. paradisiaca fruit pulp methanolic extract on body weight fasting blood glucose and oral glucose tolerance test of STZ-induced diabetes in male rats. (A) Weight change of rats, (B) Fasting blood glucose, (C) Oral glucose tolerance test. The significant differences between the means across the groups were represented within each column as * $p < 0.05$, ** $p < 0.01$, *** $p < 0.001$, ****$p < 0.0001$. ns = no significant difference at $p < 0.05$. Results are expressed as mean ± SD; n = 6.

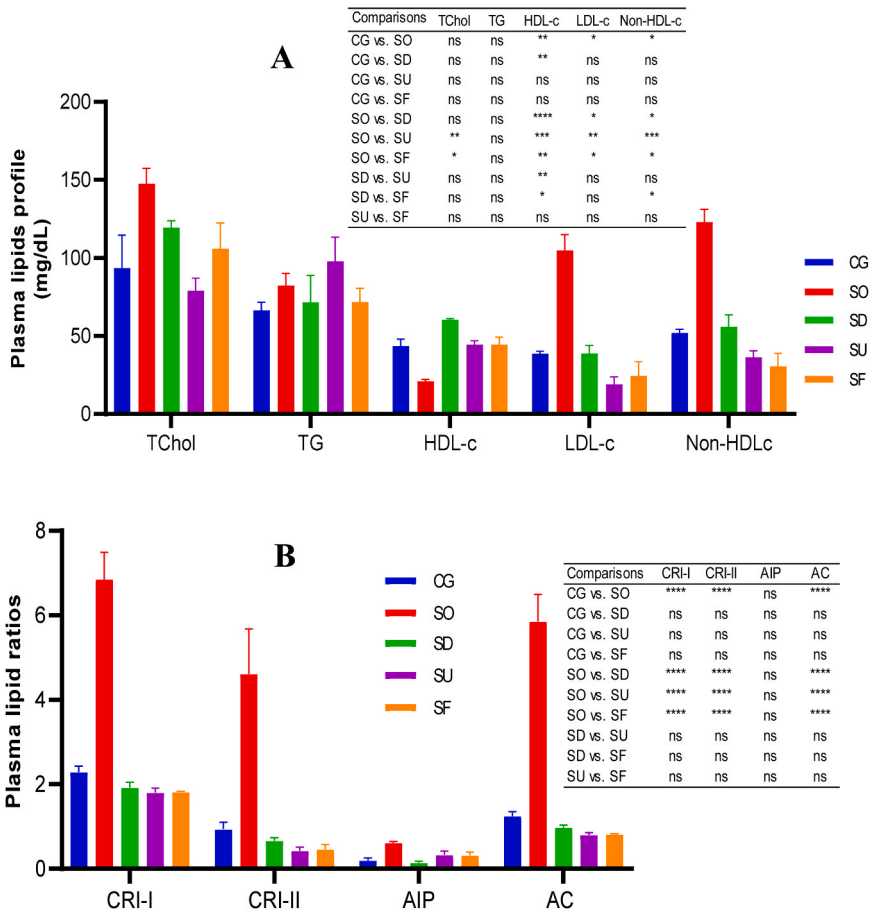


Fig. 2. Effect of fermented M. paradisiaca fruit pulp methanolic extract on plasma lipids profile and atherogenic indices of STZ-induced diabetes in male rats. (A) Plasma total cholesterol, triglycerides, high density lipoproteins, low density lipoproteins and non-high density lipids levels, (B) Plasma lipids ratios (CRI-I and II, atherogenic index of plasma and atherogenic coefficient. The significant differences between the means across the groups were represented within each column as * $p < 0.05$, ** $p < 0.01$, *** $p < 0.001$, ****$p < 0.0001$. ns = no significant difference at $p < 0.05$. Results are expressed as mean ± SD; n = 6.

non-HDL-c levels in the SO were significantly lower ($p < 0.05$) than those in the CG and treatment groups. When the treatment groups were compared with the CG, no significant change ($p > 0.05$) was observed in either LDL or non-HDL-c levels. Also, LDL-c levels within the treatment groups did not change significantly ($p > 0.05$), but the non-HDL-c level in the SF was significantly higher than in the SD ($p < 0.05$).

Regarding plasma lipid ratios (Fig. 2B), CRI-I, CRI-II, AIP and AC of SO were significantly higher ($p < 0.05$) than CG, but SD was not significantly different ($p > 0.05$) from the CG across the same parameters. In CRI-I, SU and SF were significantly lower than ($p < 0.05$) CG but not significantly different ($p > 0.05$) from the SD. The CRI-II value of SU was significantly lower ($p < .0.05$) than that of CG, but a comparison between SF and CG was not significant ($p > 0.05$). Within the diabetic group, the CRI-II of SO was significantly higher ($p < 0.05$) than in the treatment groups, whereas no significant difference ($p > 0.05$) was observed among the treatment groups. A similar comparison trend was noted within the diabetes and treatment groups in AIP and AC. While the AC comparison of SF and CG was the same as in the CRI-II, their AIP value was not significantly different ($p > 0.05$).

3.3. *Effects of fermented M. paradisiaca fruit pulp methanolic extract on pancreatic organosomatic index, insulin and protein levels, oxidative and inflammatory markers*

The pancretic organosomatic index shown in Fig. 3A shows that SD and SU were significantly ($p < 0.05$) lower than the CG, but no significant change ($p > 0.05$) was noted in SF when compared to CG. No significant difference ($p > 0.05$) was noted between the SO and treatment groups.

Fig. 3B depicts protein level in the pancreas, SO and SU had significantly lower ($p < 0.001$) protein levels when compared to the CG, whereas SF was significantly higher ($p < 0.00001$) than the CG. Within the diabetic group, SU was not significantly different from SO ($p > 0.05$), but both SD and SF were significantly different ($p < 0.05$). Within the treatment group, SF was significantly higher than both SU and SD ($p < 0.00001$), but SU was not significantly higher than SD ($p > 0.05$).

Pancreatic insulin level (Fig. 3C) in SO was significantly lower ($p < 0.0001$) than that of CG. SD and SU pancreatic insulin were not significantly different ($p > 0.05$) from CG, but SF was significantly ($p < 0.00001$) higher. In the diabetic group, pancreatic insulin in SO was significantly lower than in the other three groups. Within the treatment group, SF was significantly higher ($p < 0.00001$) than SU and SD, but SD and SU were not significantly different from each other ($p > 0.05$).

For pancreatic enzymatic oxidative stress markers (Fig. 3D), CAT, GST, and SOD activities of SO ($p < 0.05$) were significantly lower than those of the CG, but the other diabetic groups were not significantly different ($p > 0.05$) from the CG in the three enzymes. Within the diabetic group, CAT and GST activities of SO were significantly different ($p < 0.05$) from the treatment groups, but no significant change was noted in the SOD activity among the diabetic groups. Among the treatment groups, CAT and SOD activities were not altered significantly ($p > 0.05$), but GST of SD was significantly ($p < 0.05$) lower than that of

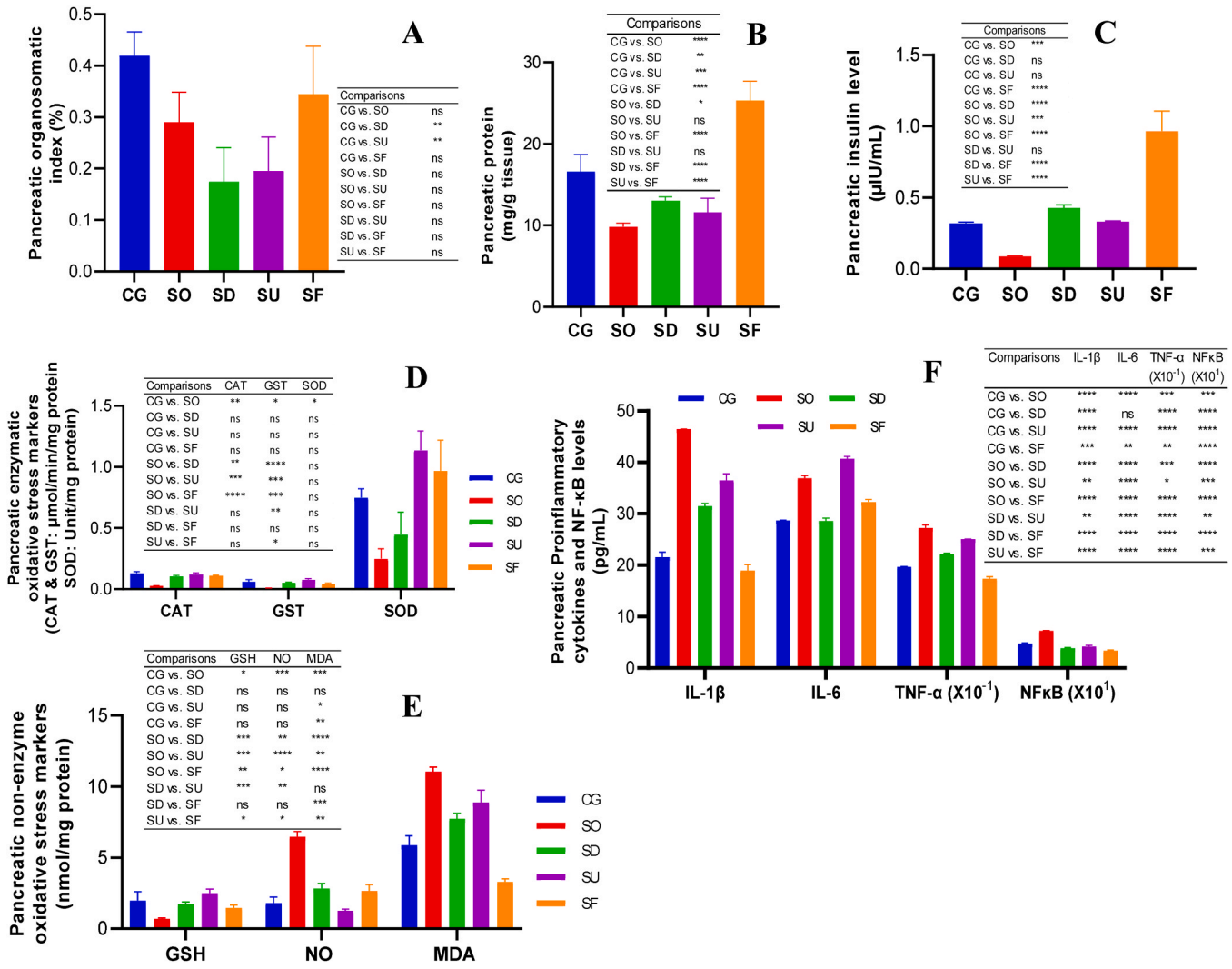


Fig. 3. Effect of fermented M. paradisiaca fruit pulp methanolic extract on pancreas somatic index, protein and insulin contents, oxidative stress and inflammatory markers of STZ-induced diabetes in male rats. (A) Pancreas organosomatic index, (B) Pancreas protein level, (C) Pancreas insulin level, (D) Pancreas enzymatic oxidative stress markers, (E) Pancreas non-enzymatic oxidative stress and lipid peroxidation markers, (F) Pancreas proinflammatory markers. The significant differences between the means across the groups were represented within each column as * $p < 0.05$, ** $p < 0.01$, *** $p < 0.001$, ****$p < 0.0001$. ns = no significant difference at $p < 0.05$. Results are expressed as mean ± SEM; n = 6.

SU.

Pancreas lipid peroxidation and non-enzymatic oxidative stress markers (Fig. 3E) showed that the GSH level in SO was significantly lower ($p < 0.05$) than in CG, while its NO and MDA were significantly higher ($p < 0.0001$). In comparison to the CG, the GSH and NO levels in SU, SD, and SF were not significantly different ($p > 0.05$). The MDA level in the treatment group compared to the CG shows that SD was not significantly different ($p > 0.05$), SU was significantly higher ($p < 0.05$), while SF was significantly lower ($p < 0.001$). In comparison to the SO, the GSH, NO, and MDA levels in the treatment groups (SD, SU and SF) were significantly different ($p < 0.001$). Within the treatment groups, GSH and NO levels in SD and SF were not significantly different ($p > 0.05$), and MDA levels in SD and SU were not significantly different ($p > 0.05$). Notably, the GSH, NO and MDA levels in SU and SF were significantly different ($p < 0.05$).

Pancreatic proinflammatory markers (Fig. 3F) showed that IL-1β level in SO, SD and SU was higher than that of CG ($p < 0.0001$), while SF was significantly lower ($p < 0.001$). All the diabetic groups were significantly different from one another ($p < 0.001$). While the treatments group were significantly lower than the SO ($p < 0.001$), SF was the least among ($p < 0.001$) among the treatments group. A similar trend was recorded in TNF-α and NF-κB SF. For IL-6 level, SO SU and SF were significantly higher than that of CG ($p < 0.001$), and SD was not significantly different from that of CG ($p > 0.05$). IL-6 level in SU was significantly higher than that of the other diabetic groups ($p < 0.00001$). While the IL-6 level in SF was significantly lower than that in SO ($p < 0.00001$), the IL-6 level in the SO group was significantly lower ($p < 0.00001$) than that in SU.

3.4. *Effects of fermented M. paradisiaca fruit pulp methanolic extract on organosomatic indices, protein, NO, GSH, and MDA in plasma, brain, and jejunum*

Fig. 4A illustrates brain and jejunum organosomatic indices. For the brain, SO value was higher ($p < 0.01$) than CG, SU and SF, with CG not differing from SD, SU, or SF ($p > 0.05$); no significant differences were observed among treatment groups ($p > 0.05$). In the jejunum, no significant ($p > 0.05$) difference was found between CG, SO and other groups. Within the *M. paradisiaca* treatment group, SF was significantly higher than SU ($p < 0.05$).

Fig. 4B presents the protein level in plasma, brain, and jejunum. Across the three tissues, SO was significantly lower ($p < 0.05$) than CG.

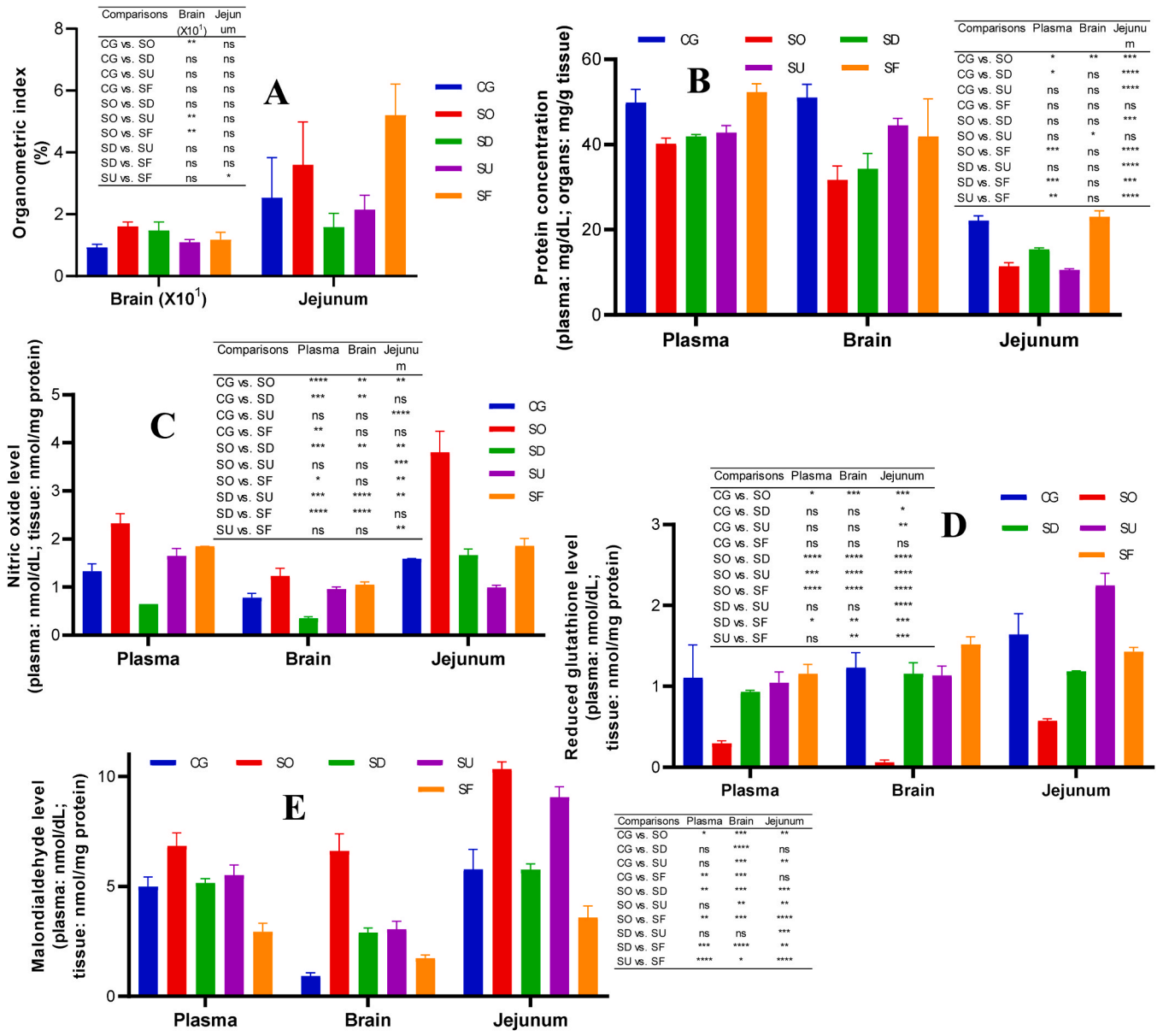


Fig. 4. Effect of fermented M. paradisiaca fruit pulp methanolic extract on organosomatic indices, protein contents, oxidative stress markers and lipid peroxidation in plasma brain and small intestine of STZ-induced diabetes in male rats. (A) Brain and small intestine organosomatic indices, (B) Plasma, brain and small intestine protein level, (C) Nitric oxide levels in plasma, brain and small intestine, (D) Reduced glutathione levels in plasma, brain and small intestine, (E) lipid peroxidation levels in plasma, brain and small intestine. The significant differences between the means across the groups were represented within each column as * $p < 0.05$, ** $p < 0.01$, *** $p < 0.001$, ****$p < 0.0001$. ns = no significant difference at $p < 0.05$. Results are expressed as mean ± SD; n = 6.

SD was lower ($p < 0.05$) than CG in the plasma and jejunum, but not statistically different ($p > 0.05$) in the brain. The protein level in the SF was not significantly different from that in the CG in the three tissues. A comparison between SO and the treatment groups showed that SD was not different ($p > 0.05$) from SO in the plasma and brain, but was significantly ($p < 0.0001$) higher in the jejunum. When compared across the three tissues, SU was significantly higher ($p < 0.05$) than SO in the brain only. Between SO and SF, a significant increase ($p < 0.0001$) was noted in the plasma and jejunum. Within the *M. paradisiaca* treatment groups, SU was significantly ($p < 0.00001$) higher in the jejunum only. SF was significantly higher than SD and SU in both plasma and the jejunum, but not in the brain ($p > 0.05$).

The nitric oxide (NO) level (Fig. 4C) in the plasma, brain and jejunum of SO was significantly higher ($p < 0.001$) than that of CG. NO in the plasma and brain of SD was significantly lower ($p < 0.001$) than in CG, but not ($p > 0.05$) in the jejunum, which was comparable to that of CG. The NO level in the plasma and brain of SU was not significantly different ($p > 0.05$) from that of the CG, but in the jejunum, SU was significantly lower ($p < 0.00001$). Between CG and SF, plasma NO was significantly higher ($p < 0.001$), but no change ($p > 0.05$) was noted in the brain and jejunum. The NO level comparison between SO and SD showed that SD was significantly lower ($p < 0.001$) in the three tissues; between SO and SU, SU was not different ($p > 0.05$) from SO in plasma and brain, but lower ($p < 0.0001$) in the jejunum. Between SO and SF, SF was significantly lower ($p < 0.05$) in plasma and jejunum, but no significant change ($p > 0.05$) was observed in the brain. Among the treatment groups, SD was significantly lower ($p < 0.0001$) than SF and SU in the three tissues, except in the jejunum of SF, where SU was significantly lower ($p < 0.01$) than SD, but SD and SF were not significantly different ($p > 0.05$). Between SU and SF, a significant difference was noted ($p < 0.01$) in the jejunum only.

Fig. 4D shows reduced glutathione (GSH) levels. In the plasma, brain

and jejunum of SO, GSH level was significantly lower ($p < 0.05$) than that of CG and other groups. The GSH level in plasma and brain of SD, SU and SF was not significantly ($p > 0.05$) different from the CG, but in the jejunum, SD and SU were significantly lower ($p < 0.05$) and higher ($p < 0.01$), respectively, when compared to CG. Between the SF and CG, no significant difference ($p > 0.05$) was noted. Also, no significant difference was noted in the plasma and brain of SD and SU ($p < 0.05$), but was significantly higher in the jejunum ($p < 0.00001$). Between SD and SF, SF was significantly higher ($p < 0.05$) across the three tissues. When SU and SF were compared, SF was higher ($p < 0.001$) in the brain, while SU was higher ($p < 0.001$) in the jejunum, but no difference in the plasma ($p > 0.05$).

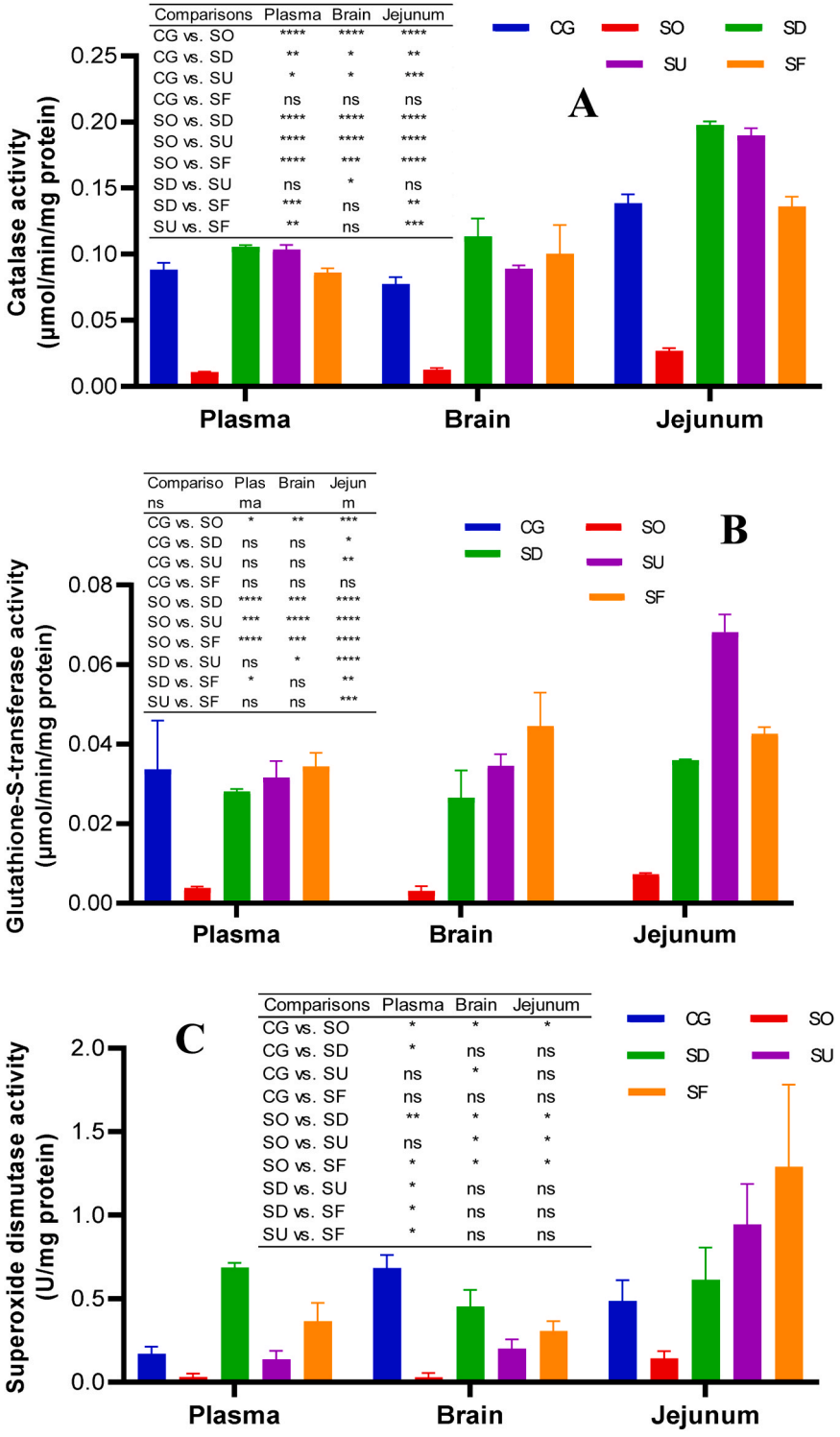


Fig. 5. Effect of fermented M. paradisiaca fruit pulp methanolic extract on selected enzymatic oxidative stress markers in plasma, brain, and jejunum of STZ-induced diabetes in male rats. (A) Catalase activity in plasma, brain and small intestine, (B) Glutathione-S-transferase activity in plasma, brain and small intestine, (C) Superoxide dismutase activity in plasma, brain and small intestine. The significant differences between the means across the groups were represented within each column as * $p < 0.05$, ** $p < 0.01$, *** $p < 0.001$, ****$p < 0.0001$. ns = no significant difference at $p < 0.05$. Results are expressed as mean ± SD; n = 6.

Fig. 4E presents lipid peroxidation (MDA) levels. MDA level in the plasma, brain and jejunum of SO was significantly higher ($p < 0.05$) than CG, SD and SF. A comparison between SO and SU showed that SU was significantly lower ($p < 0.001$) in the brain and jejunum but not significant ($p > 0.05$) in the plasma. A comparison between SD and CG revealed a significant increase ($p < 0.00001$) in the brain only. Between SU and CG, SU showed a significant elevation ($p < 0.001$) in both the brain and jejunum, but no change ($p > 0.05$) in the plasma. Between the SD and SU, a significant ($p < 0.0001$) difference was noted in the jejunum only. SF, on the other hand, was significantly ($p < 0.05$) lower than both SU and SD across the three tissues.

3.5. Effects of fermented *M. paradisiaca* fruit pulp methanolic extract on enzymatic oxidative stress markers

Catalase (CAT) activity in plasma, brain, and jejunum is shown in Fig. 5A. The CAT activity in the plasma, brain and jejunum of SO was significantly lower ($p < 0.0001$) than that of CG and other diabetic groups. A comparison between the CG and diabetes treatment groups showed that CAT activity in SU and SD was significantly higher ($p < 0.05$) across the three tissues; however, SF was not significantly different ($p > 0.05$) in any of the tissues compared to CG. Within the treatment groups, CAT activity in plasma and jejunum of SD and SU was not significantly ($p > 0.05$) different, but SD was significantly higher ($p < 0.05$) in the brain. SF was significantly lower ($p < 0.05$) than both SD and SU in the plasma and jejunum, but not significantly different in the brain.

Fig. 5B presents glutathione-S-transferase (GST) activity. In plasma, brain and jejunum, SO was significantly lower ($p < 0.05$) than in CG and other diabetic groups. No significant difference ($p > 0.05$) was noted between CG, SU, SD and SF in plasma and brain, but in the jejunum, the GST activity of SD and SU was significantly ($p < 0.05$) lower and higher, respectively, than that of the CG. While SF was not significantly different ($p > 0.05$) from the CG in the plasma and other tissues. The GST activity in the plasma of SD and SU was not significantly different ($p > 0.05$) from each other, but in the brain and jejunum. Between SD and SF, GST activity was significantly higher ($p < 0.05$) in the plasma and jejunum of SF but not significantly different ($P > 0.05$) in the brain. No significant change was noted between SU and SF in the plasma and brain, but SU was significantly higher ($p < 0.0001$) in the jejunum.

Fig. 5C shows superoxide dismutase (SOD) activity. SOD activity of SO was significantly lower in the brain, plasma and jejunum ($p < 0.05$) when compared to CG. When the SD, SU and SF were compared to CG, the SF showed no significant difference across the three tissues. Whereas, SU and SD showed no significant change ($p > 0.05$) in the jejunum. In the plasma, SD was significantly higher ($p < 0.05$), but SU was significantly lower ($p < 0.05$) than CG. In the brain, SU was significantly lower, while SD did not show a significant change in SOD activity. The comparison between SO and the treatment groups showed that SD and SF were significantly higher ($p < 0.05$) than SO in the three tissues. SU was significantly higher than SO in the jejunum and brain but not significant ($p > 0.05$) in the plasma. Within the treatment groups, no significant difference ($p > 0.05$) was observed in the brain and jejunum. In the plasma, the three groups were significantly different ($p < 0.05$) from one another.

3.6. Effects of fermented *M. paradisiaca* fruit pulp methanolic extract on acetylcholinesterase and Na^+/K^+- ATPase activities in the brain

Acetylcholinesterase (AChE) and Na^+/K^+- ATPase activities in the brain are shown in Table 1. No significant differences were noted in the enzyme activities when compared with the CG ($p > 0.05$). However, there were marked differences across the treatment group when compared in terms of percentage change. For AChE activity, diabetes alone (SO) resulted in a marked reduction (−25.59%) compared to CG. The unfermented extract (SU) caused an increase in AChE activity (29.98%), while the fermented extract (SF) led to a moderate elevation (19.76%). Also, Na^+/K^+-ATPase activity of the SO group showed a pronounced decrease (−23.95%) relative to CG. Glibenclamide (SD) produced a slight increase (10.93%). SU enhanced the enzyme activity above control (25.10%), whereas SF reduced it (−11.74%), though to a lesser extent than the untreated diabetic group.

Table 1
Effects of fermented *M. paradisiaca* fruit pulp methanolic extract on acetylcholine esterase and Na^+/K^+- ATPase activities in the brain.

	AChE activity (nmol/min/mg protein)	AChE activity change from CG (%)	Na^+/K^+-ATPase activity (nmol Pi/min/mg protein)	Na^+/K^+-ATPase changes from CG (%)
CG	21.37 ± 2.84	0.00	13.91 ± 2.30	0.00
SO	15.90 ± 0.66	−25.59	10.65 ± 0.51	−23.95
SD	21.36 ± 4.26	−0.06	13.27 ± 2.03	10.93
SU	27.78 ± 2.21	29.98	14.59 ± 0.42	25.10
SF	25.59 ± 5.02	19.76	12.28 ± 0.93	−11.74

Data are presented as mean ± standard deviation (mean±SD) for $n = 6$ per group. Statistical comparisons between the control group and treatment group were performed. Significance levels are indicated as $^*p < 0.05$

3.7. Effects of fermented *M. paradisiaca* fruit pulp methanolic extract on pancreatic islet morphometry

Fig. 6 shows a representative H&E-stained micrograph and histomorphometry chart. The CG shows islets with well-defined round architecture and a dense core of endocrine cells, while the × 400 inset reveals tightly packed endocrine cells with evenly distributed, round nuclei, minimal cytoplasmic vacuolation, and almost absence of inflammatory cell infiltration. In the SO, the islets exhibited marked shrinkage, dispersed nuclei, increased pyknotic nuclei, irregular perimeters, and abundant inflammatory infiltrates. The SO inset demonstrates pronounced cellular degeneration characterised by dispersed and shrunken endocrine cells, numerous darkly stained pyknotic nuclei, cytoplasmic vacuolization, and dense inflammatory infiltrates within and around the islet tissue. Treatment with glibenclamide (SD) and unfermented extract (SU) partially restores islet morphology. This is more evident in their respective insets as both show improved cellular organisation compared with SO, with fewer pyknotic nuclei and reduced inflammatory infiltration. The SF achieves near-normal islet size, compact nuclear distribution, reduced pyknotic cells, smoother perimeters, and minimal inflammation, and the inset shows densely packed endocrine cells with predominantly round, lightly stained nuclei, minimal cytoplasmic vacuolation, and scarce inflammatory cells. The morphometry chart indicates that the nuclei density in the CG is significantly higher than in SO and SU only ($p < 0.001$ and $p < 0.05$, respectively). Among the diabetes group, SO is significantly lower than the other three. For the islet perimeter values, CG was significantly higher than the SO ($p < 0.05$) and SD ($p < 0.001$) only. Among the diabetes groups, no significant difference was found between the SO and SD ($p > 0.05$), but SU and SF were significantly higher than the SO ($p < 005$). For the inflammatory cells and vacoule counts, SO was significantly higher than CG and the treatment groups, except for the SD, which showed no significant difference in its inflammatory cell count ($p > 0.05$).

3.8. Effects of fermented *M. paradisiaca* fruit pulp methanolic extract on pancreatic islet (β-Cell granules)

Fig. 7 is representative of × 400 magnification Gomori aldehyde-fuchsin (AF) stained micrographs and their histomorphometry chart. In the CG, the islets are well delineated and exhibit intense, homogeneous dark staining within the endocrine cell population, reflecting a high abundance and uniform distribution of AF-positive cytoplasmic

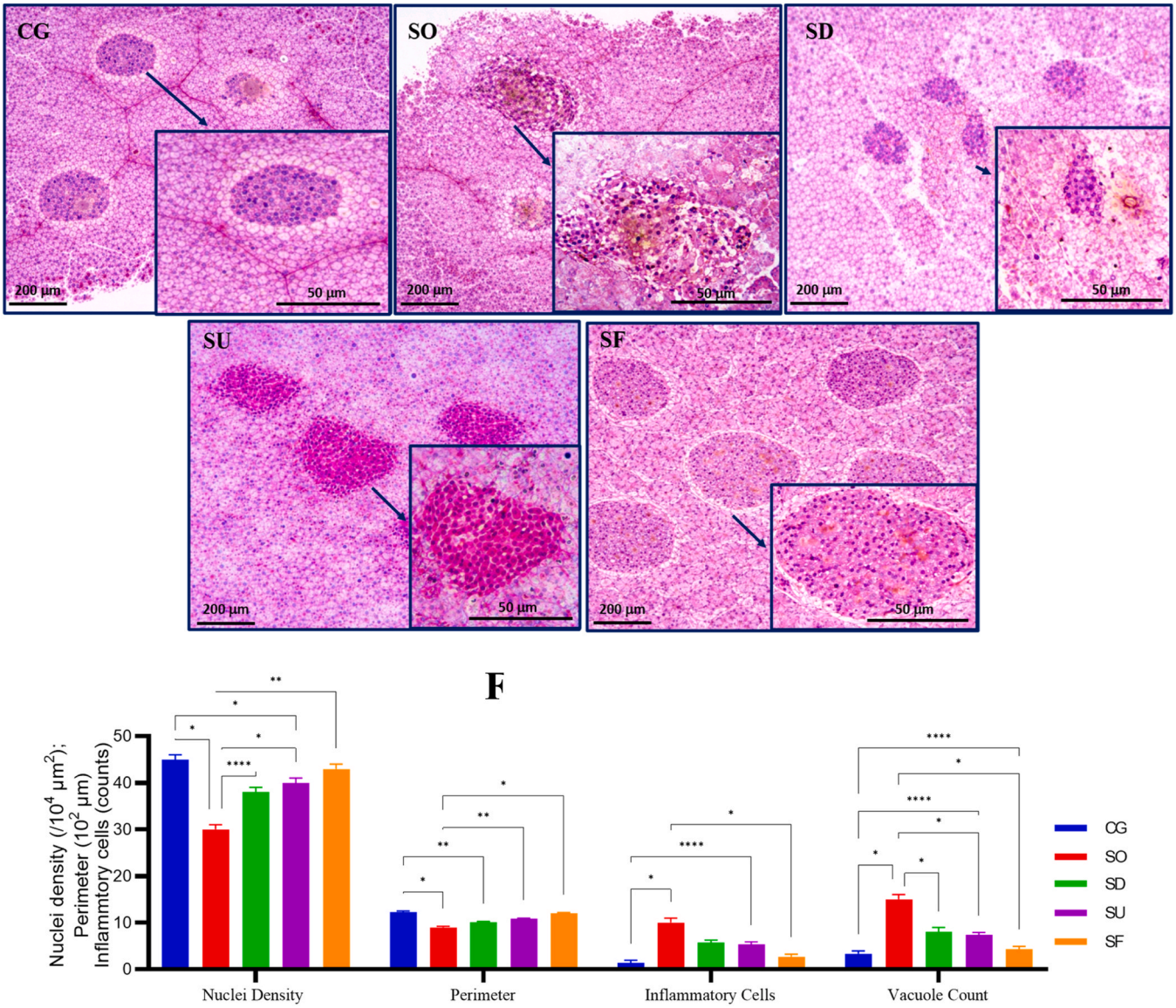


Fig. 6. Effect of fermented M. paradisiaca fruit pulp methanolic extract on pancreatic islet histomorphology in streptozotocin (STZ)-induced diabetic male rats. Representative photomicrographs of Hematoxylin and Eosin (H&E)–stained pancreatic sections from the experimental groups: CG, control group; SO, STZ-only group; SD, STZ + glibenclamide–treated group; SU, STZ + unfermented M. paradisiaca fruit pulp methanolic extract–treated group; SF, STZ + fermented M. paradisiaca fruit pulp methanolic extract–treated group. Low-magnification images (×100) illustrate the general distribution and architecture of the islets of Langerhans within the pancreatic parenchyma. Insets (high magnification, ×100) highlight islet cellularity and structural details, with arrows indicating representative islets. Scale bars: 200 µm (main panels) and 50 µm (insets). (F) Semi-quantitative/quantitative scoring of pancreatic histomorphological parameters derived from H&E-stained micrographs across CG, SO, SD, SU, and SF groups, presented as comparative bar graphs. The significant differences between the means across the groups were represented as * $p < 0.05$, ** $p < 0.01$, *** $p < 0.001$, ****$p < 0.0001$. ns = no significant difference at $p < 0.05$. Results are expressed as mean ± SD; n = 3.

granules with preserved cellular density and architecture. The SO shows some markedly diminished AF-positive intensity, denoting substantial loss of AF-positive granules and compromised morphology within the pale islet areas, reduced cellular compactness, and irregular islet boundaries. The SD panel shows partial AF-positive staining characteristics, with a moderate increase in darkly stained cells and a more discernible islet outline compared with SO. In the SU panel, AF-positive granule density was comparatively higher than SO, with improved uniformity of stained regions, and better structural cohesion. The SF panel showed relatively uniform AF-positive granules, which are characterised by a well-coordinated, distributed cellular organisation, clearer islet definition, and morphological integrity than the SU.

Morphometry estimation of the AF-stained plate showed that mean islet density and islet-border integrity of the SO ($p < 0.05$) were significantly lower than the CG, but the treatment groups were not significantly different ($p > 0.05$) from the CG. Between the diabetes group, SO was significantly ($p < 0.05$) lower than the other three groups. The estimated islet area of the diabetes rats group was significantly lower ($p < 0.05$) than the CG, except for the SF, which was not significantly different. Also, a comparison within the diabetes group shows that SO is significantly lower than the other three. When the aldehyde-positive area of the islet of SO was compared with the CG, SO was significantly lower ($p > 0.05$). For the percentage vacuolation, the SO and SD were significantly higher ($p < 0.05$) than both CG, SU and SF. When SD and SO were compared, SO was significantly higher ($p < 0.05$). Regarding the non-endocrine area, no significant difference ($p > 0.05$) was noted between the CG and all the diabetes groups. But SF was significantly lower ($p < 0.05$) than the SO group.

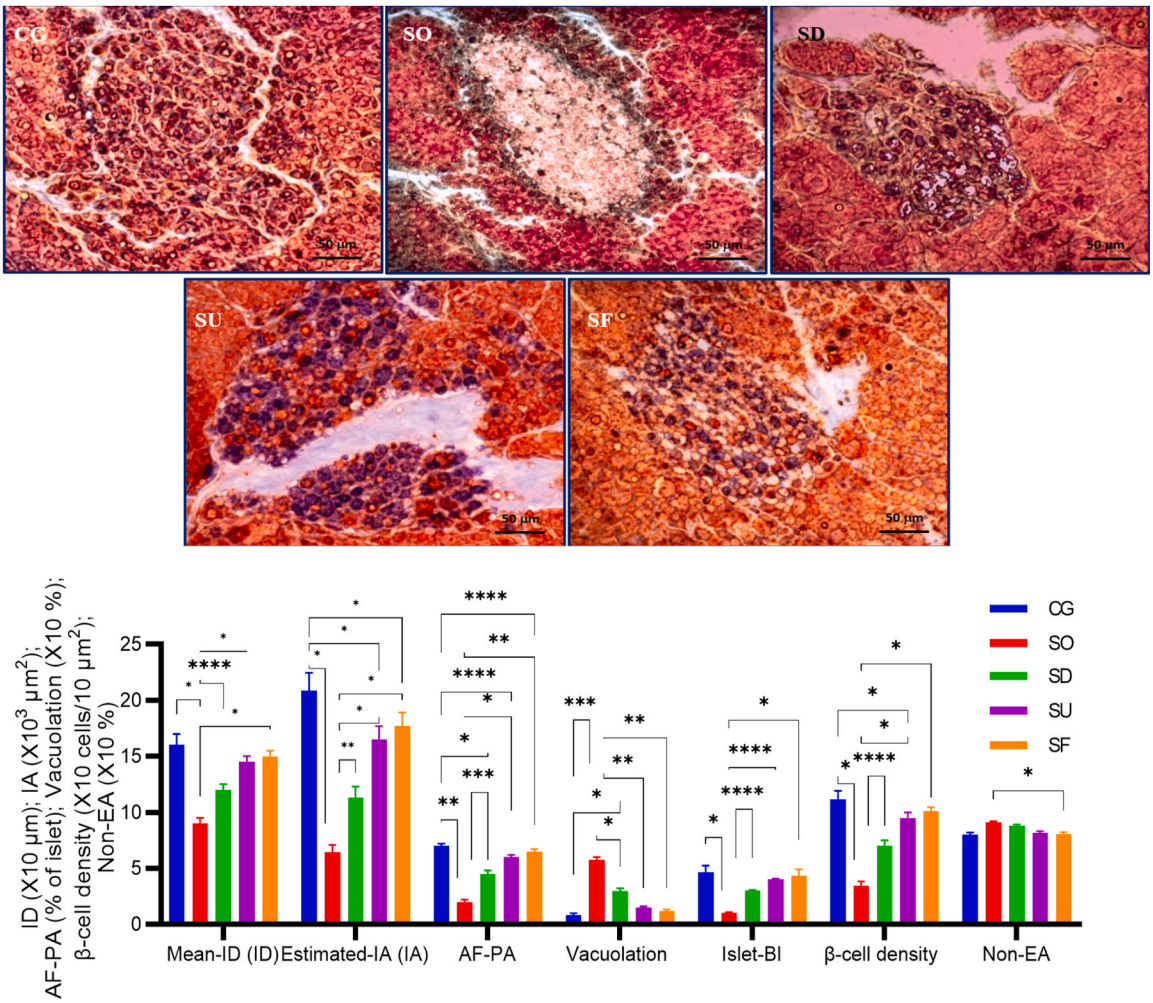


Fig. 7. Effect of fermented M. paradisiaca fruit pulp methanolic extract on pancreatic islet histoarchitecture in streptozotocin (STZ)-induced diabetic male rats, as assessed by Gomori aldehyde–fuchsin staining. *Representative photomicrographs of pancreatic sections from the experimental groups: CG, control group; SO, STZ-only group; SD, STZ + glibenclamide–treated group; SU, STZ + unfermented M. paradisiaca fruit pulp methanolic extract–treated group; SF, STZ + fermented M. paradisiaca fruit pulp methanolic extract–treated group. Images (×40) illustrate the distribution and staining characteristics of islet cells within the pancreatic parenchyma. Scale bar = 50 µm. (F) Semi-quantitative/quantitative scoring analysis of Gomori aldehyde–fuchsin–stained pancreatic islet micrographs from CG, SO, SD, SU, and SF groups, presented as comparative bar graphs.* (F) Semi-quantitative/quantitative scoring of pancreatic histomorphological parameters derived from H&E-stained micrographs across CG, SO, SD, SU, and SF groups, presented as comparative bar graphs. Morphometry abbreviations: Mean islet diameter (Mena-ID), Estimated islet area (Estimated-IA), AF-positive area (AF-PA), Vacuolation, Islet border integrity (Islet-BI) and Non-endocrine area in field (Non-EA). The significant differences between the means across the groups were represented as * $p < 0.05$, ** $p < 0.01$, *** $p < 0.001$, ****$p < 0.0001$. ns = no significant difference at $p < 0.05$. Results are expressed as mean ± SD; n = 3.

3.9. *Effects of fermented M. paradisiaca fruit pulp methanolic extract on hypothalamic morphometry and pathology*

Fig. 8 represents H&E-stained micrographs (×40) of the anterior hypothalamus, including the paraventricular (PCN), suprachiasmatic (SCN), and supraoptic (SON) nuclei, demonstrating that CG retained uniform neuronal size and intact nuclear morphology, with no evidence of vacuolation or inflammatory infiltrates. By contrast, SO displayed shrunken, angular neurons accompanied by widespread vacuole formation, increased pyknotic nuclei, and focal inflammatory cell clusters. Intervention with glibenclamide (SD) yields a partial morphological rescue: fewer and smaller vacuoles and reduced pyknosis are evident, although mild gliosis persists. In SU, neuronal architecture is moderately preserved, with only occasional vacuoles and scattered pyknotic profiles. Impressively, the SF exhibits near-normal cytoarchitecture, characterised by minimal vacuolation and rare pyknotic or inflammatory cells. On the quantitative analysis, the total hypothalamic region cell density analysis revealed that CG neurons were more sparsely packed than in experimental groups ($p < 0.01$). SO density was lower than in SD and SU ($p < 0.05$) and markedly lower than SF ($p < 0.0001$). Although SD and SU densities were comparable ($p > 0.05$), both were significantly reduced relative to SF ($p < 0.05$). For vacuole counts, CG exhibited the fewest vacuoles compared to SO and other diabetic groups ($p < 0.05$); SO counts exceeded SD, SU and SF ($p < 0.05$); while SD, SU, and SF did not differ significantly ($p > 0.05$).

3.10. *Effects of fermented M. paradisiaca fruit pulp methanolic extract on hypothalamic vacuolation (magnified view)*

As illustrated in Fig. 9, H&E-stained (×400) coronal sections from the anterior hypothalamus at the level of the suprachiasmatic region (H&E, ×400) demonstrate clear group-dependent morphological differences when the CG panel is used as the normal reference. The CG shows preserved cytoarchitecture, with uniformly sized neuronal cell bodies exhibiting consistent cytoplasmic eosinophilia, round to oval nuclei with evenly distributed chromatin, and a compact, homogeneous neuropil containing regularly dispersed small glial-type nuclei.

The SO panel displays the most pronounced pathological alterations

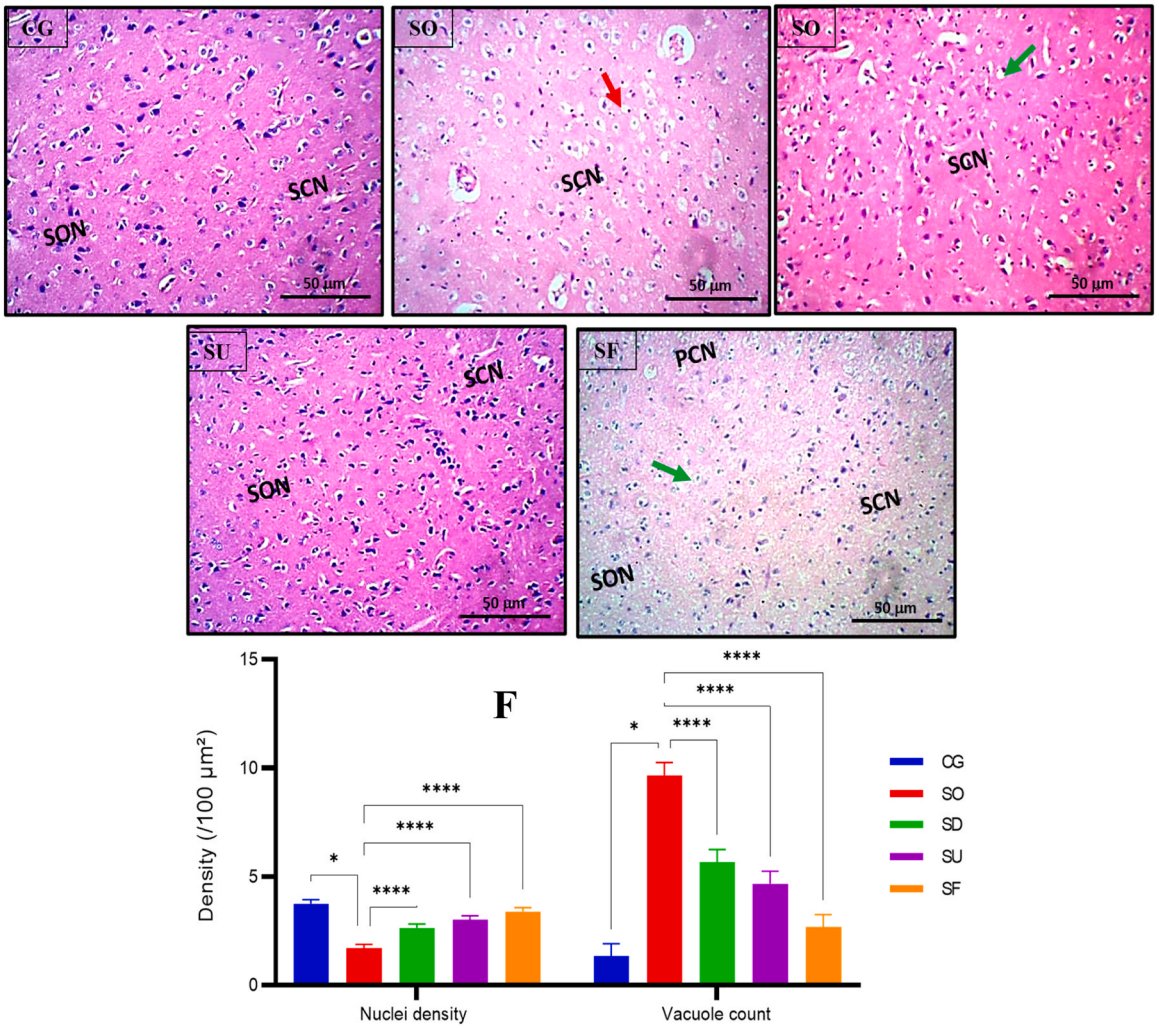


Fig. 8. Effect of fermented M. paradisiaca fruit pulp methanolic extract on hypothalamic histomorphology in streptozotocin (STZ)-induced diabetic male rats. *Representative low-magnification photomicrographs (Hematoxylin and Eosin staining, ×40) of the of the anterior hypothalamus (suprachiasmatic region) of rats. Groups: CG, control group; SO, STZ-only group; SD, STZ + glibenclamide–treated group; SU, STZ + unfermented M. paradisiaca fruit pulp methanolic extract–treated group; SF, STZ + fermented M. paradisiaca fruit pulp methanolic extract–treated group. Sections illustrate neuronal organization within the supraoptic nucleus (SON), suprachiasmatic nucleus (SCN), and periventricular/adjacent hypothalamic regions as indicated. In the SO group, altered neuronal morphology and neuropathological features are indicated by arrows, whereas treatment groups (SD, SU, and SF) show relative preservation of hypothalamic cytoarchitecture. Scale bar = 50 µm. (F) Semi-quantitative/quantitative scoring analysis of H&E-stained hypothalamic micrographs from CG, SO, SD, SU, and SF groups, presented as comparative bar plots.* The significant differences between the means across the groups were represented as * $p < 0.05$, ** $p < 0.01$, *** $p < 0.001$, ****$p < 0.0001$. ns = no significant difference at $p < 0.05$. Results are expressed as mean ± SD; n = 3.

relative to CG, characterised by frequent neuronal cytoplasmic pallor, prominent pericellular clearing, increased numbers of darkly stained, condensed nuclei, and a loosened, heterogeneous neuropil with focal rarefaction. Among the treatment groups, distinct inter-group differences are evident. The SD panel shows partial attenuation of the SO-associated changes, with mixed neuronal morphology characterised by variable cytoplasmic staining intensity and persistent pericellular clearing; scattered pyknotic nuclei remain frequent, and the neuropil demonstrates uneven density. In comparison, the SU panel exhibits a denser cellular arrangement than SD, with fewer overtly pale neuronal profiles and more uniform cytoplasmic eosinophilia. Although small hyperchromatic nuclei are prominent, the neuropil appears comparatively compact, and degenerative nuclear features are less conspicuous than in SD. The SF panel differs from both SD and SU by displaying more prominent neuronal cell bodies with pale to moderate cytoplasmic staining and round nuclei of variable chromasia, set within neuropil showing focal rarefaction; however, the frequency of pyknotic nuclei appears lower than in SD and is comparable to or less than that observed in SU. Overall, while all treatment groups show improved neuronal preservation relative to the untreated injury group, SD retains the greatest degree of morphological heterogeneity and degenerative features, whereas SU demonstrates the most compact cellular organisation, and SF is distinguished by more conspicuous neuronal profiles with intermediate preservation of neuropil integrity, none fully recapitulating the uniform appearance of the normal control at the examined magnification.

3.11. *Effects of fermented M. paradisiaca fruit pulp methanolic extract on jejunum morphometry and pathology*

Fig. 10 presents representative low-magnification photomicrographs of jejunal sections of rats. In the CG, the jejunum exhibited a well-preserved architecture characterised by tall, closely packed villi with intact epithelial lining, orderly crypt arrangement, and a clearly defined mucosa–submucosa interface, reflecting normal intestinal morphology. The SO showed marked disrupted histoarchitecture, evidenced by apparent villus shortening and blunting, irregular villus spacing, and disorganisation of the crypt–villus axis, indicating intestinal injury.

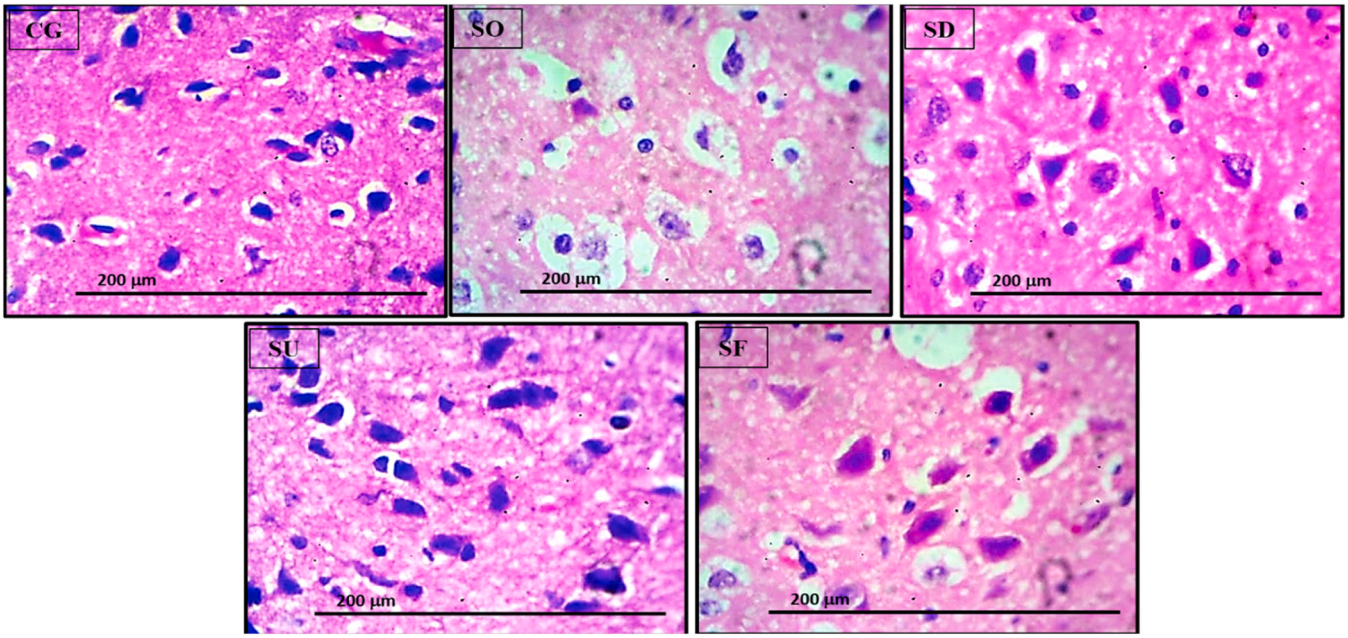


Fig. 9. Effect of fermented Musa paradisiaca fruit pulp methanolic extract on hypothalamic cytoarchitecture in streptozotocin (STZ)-induced diabetic male rats. Representative high-magnification photomicrographs (Hematoxylin and Eosin staining, ×400) of of the anterior hypothalamus (suprachiasmatic region) of rats. Groups: CG, control group; SO, STZ-only group; SD, STZ + glibenclamide–treated group; SU, STZ + unfermented M. paradisiaca fruit pulp methanolic extract–treated group; SF, STZ + fermented M. paradisiaca fruit pulp methanolic extract–treated group. Images depict neuronal cell bodies and surrounding neuropil. The SO group shows marked alterations in neuronal morphology compared with the CG, whereas treatment with glibenclamide, unfermented, or fermented M. paradisiaca pulp extracts is associated with relative preservation of neuronal structure. Scale bar = 200 µm.

Contrary to the SO, the treatment group, SD, partially showed noticeable improvement in villus length and alignment. Although the mucosal organisation did not fully resemble that of the CG. Also, the SU showed a jejunal structure with residual irregularities in villi and crypts morphology than the SO. SF exhibited elongated and uniformly arranged villi, clearer crypt architecture, and overall mucosal organisation approaching that observed in the CG. Histomorphometrically, the villus height of the CG was significantly higher ($p < 0.05$) than both SO, SD and SU but not significantly ($p > 0.05$) different from the SF. Among the diabetes groups, SO and SU were significantly lower ($p < 0.05$) than SD and SF, but no significant difference ($p > 0.05$) was observed between SO and SU. For the crypt depth, SO is significantly higher ($p < 0.05$) than both CG and the treatment groups. Also, the crypt depth of the SU was significantly higher ($p < 0.05$) than CG, but SD and SF were not significantly different ($p > 0.05$) from CG. The villus height to crypt ratio (VH: CD) of all the diabetes groups was significantly ($p < 0.05$) lower than CG.among the diabetes groups, SO had a significantly ($p < 0.05$) VH:CD than the rest. The villus width variation across all groups was the same trend as that of the VH:CD. Also, villus density and total mucosal thickness variations across all the groups had the exact trend recorded, but in a reverse pattern. That is, while the crypt depth of the CG and treatment groups was lower than the SO, the villus density and total mucosal thickness of these groups were higher. The exception noted in these trends was that, contrary to the crypt depth, SD was significantly lower than CG in both villus density and total mucosal thickness, and no significant difference was noted between SO and SU in villus density.

4. Discussion

This study revealed that STZ-induced β-cell destruction precipitates systemic metabolic derangements, manifesting as weight loss and hyperglycaemia. This exacerbates dyslipidaemia and elevates atherogenic indices, which further depict pancreatic redox dyshomeostasis and inflammatory conditions.

STZ-induced diabetes (SO) precipitated rapid weight loss by day 7 (Fig. 1A). This observation reflects insulin deficiency-driven proteolysis (proteinuria) and enhanced gluconeogenesis [58,59], which is a consequence of glucosuria [58]. Both unfermented (SU) and fermented (SF) *M. paradisiaca* fruit pulp extracts moderate body weight better than glibenclamide. However, only SF restored weight to near control level as early as day 14. The distinctive weight-moderating effect of SF may be ascribed to some of the constituents, like short-chain fatty acids (SCFAs) and modified phenolic compounds, which are unique to fermented *M. paradisiaca* (plantain) fruit pulp extract (*f*-PUME), as identified in our previous works [22,23]. Numerous studies have shown that SCFAs modulate body weight in various metabolic energy (pathological) conditions. For example, Anachad et al. [60] reported that SCFA prevents obesity in T2DM conditions, while Wen et al. [61] showed that dietary SCFA intervention in (STZ-induced) T1DM in mice prevents weight loss.

In fasting glycaemia (Fig. 1B), the greater reductions elicited by *f*-PUME (SF)over *u*-PUME (SU) or glibenclamide (SD) from day 14 onward aligned with our in-vitro study, which showed that *f*-PUME possesses greater inhibitory potential against α-amylase [22], which may suggest a possible mechanism that *f*-PUME employs to fight against DM. Additionally, the synergistic effects of some of the phytochemical constituents [62,63] and other unique components in the fermented extracts [22,23,25] might have potentiated *f*-PUME efficacy against hyperglycaemia. Consequently, contributing to the outcome observed on OGTT (Fig. 1C), as SF markedly blunted the hyperglycaemia peak within the 30–60 min and quickly returned toward baseline.

The compounding and consequential effects of STZ-induced DM on the plasma lipid profile and atherogenic indices are well documented [64–67]. As shown in this study, the SO group showed all the high-risk factors. Although TChol and TG remained stable across all the intervention groups, they showed diverse and intriguing patterns of hypolipidemic effects (Fig. 2A & B). For example, unfermented extract (SU) could not suppress plasma TG and yet had the least LDL-c, even at a level lower than the CG, by effectively suppressing plasma TChol. *f*-PUME, on its part, moderately suppressed TChol and TG, and stabilised HDL-c

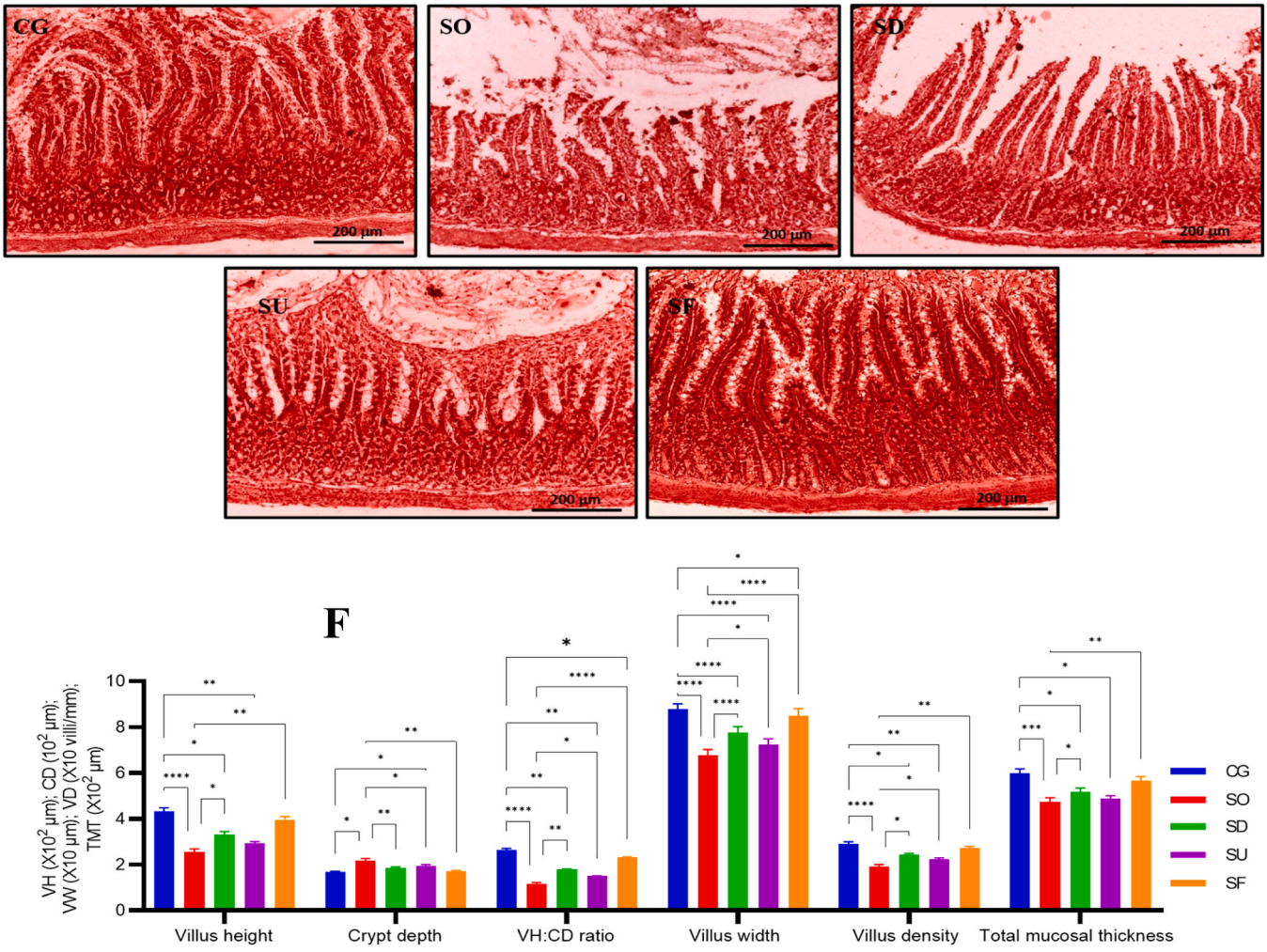


Fig. 10. Effect of fermented Musa paradisiaca fruit pulp methanolic extract on jejunal histomorphology in streptozotocin (STZ)-induced diabetic male rats. Representative low-magnification photomicrographs of jejunal sections from male rats stained with hematoxylin and eosin (H&E, ×40). The experimental groups are shown as follows: CG, control group; SO, streptozotocin (STZ)–only group; SD, STZ + glibenclamide–treated group; SU, STZ + unfermented M. paradisiaca fruit pulp methanolic extract–treated group; SF, STZ + fermented M. paradisiaca fruit pulp methanolic extract–treated group. Panels illustrate overall mucosal architecture, highlighting villus height and density, crypt organization, epithelial integrity, and lamina propria cellularity. Scale bar = 200 µm.(F) Quantitative/semi-quantitative analysis of jejunal histomorphological parameters derived from the H&E-stained sections of CG, SO, SD, SU, and SP groups, presented as group-wise comparisons in the bar chart. Data reflect treatment-associated differences in jejunal mucosal structure following STZ-induced diabetic injury. The significant differences between the means across the groups were represented as * $p < 0.05$, ** $p < 0.01$, *** $p < 0.001$, ****$p < 0.0001$. ns = no significant difference at $p < 0.05$. Results are expressed as mean ± SD; n = 3.

levels to the level observed in the control rat group. In diabetic conditions, dyslipidemia promotes atherogenesis and coronary heart disease, but the plasma lipid components may not independently reflect the angiographic risk indices[68]. Hence, derived lipid indices such as Castelli Risk Indices I/II (CRI-I and CRI-II), Atherogenic Index of Plasma (AIP), and Atherogenic Coefficient (AC), which better integrate the pro- and anti-atherogenic coronary components, become essential. This is because they reveal stronger associations with subclinical atherosclerosis and cardiovascular outcomes, and offer superior risk stratification [68,69]. In this study, the TG and TChol levels of the SO group appear normal; however, the derived lipid indices showed that STZ-induced dyslipidemia may increase both coronary heart disease and atherogenic risk factors (CRI-I, CRI-II, AIP, and AC) up to 3–fold in a diabetic condition. On the contrary, both interventions (*u*-PUME and *f*-PUME) in this work suppressed both the atherogenic and coronary risk indices, indicating cardioprotective potential [25,63,70]. Among other lipidemic indices, non-HDL-c is considered a reference factor for diabetes-induced coronary heart disease (CHD) because of its unconditional and independent association with CHD in diabetic conditions [69]. Notably, plasma lipids normalisation observed in fermented *M. paradisiaca* methanolic extract-treated diabetic rats is not unprecedented, as some of the ^{1}H NMR identified compounds [22], such as coriolic acid (an antilipidemic compound), have been reported to be directly involved in cholesterogenesis inhibition and atherosclerosis suppression via the linoleic acid metabolism pathway.

The assessment of pancreatic organosomatic index, protein content, insulin levels, oxidative stress markers, and inflammatory mediators provides critical insight into the structural and functional integrity of the pancreas under diabetic conditions and therapeutic interventions [71–75]. While these functional and structural indices were impaired in the SO group in our study, diverse effects were observed across the intervention groups. Only SF restored pancreatic weight and protein level compared to control, outperforming the unfermented and drug treatment groups. According to Lhoste et al. [76], pancreatic function and protein levels, especially proteolytic enzymes in pancreatic juice, are primarily influenced by fermentation, and it was observed that SCFA are the drivers of these effects. A similar induction by SCFA might account for the elevated pancreatic protein and the partial increase in the

organosomatic index recorded in the SF group, as shown in this study. Iyoriobhe et al. [77] reported that protein isolated from fermented melon seeds promotes pancreas protein concentration.

Furthermore, pancreatic proteins and insulin levels may be mutually inclusive, because insulin secretion is largely glycemic-dependent. However, the increase in pancreatic proteins and insulin levels might be directly or indirectly attributed to the other components of *f*-PUME present in the SF rats. It is noteworthy to state that both glibenclamide and unfermented *M. paradisiaca* fruit pulp extract stimulated pancreatic insulin secretion, but not pancreatic protein, in this work. The insulin level in the SF was more than two-fold that of the control group, suggesting that fermented *M. paradisiaca* fruit pulp extract performs better than the other interventions.

ROS generation in the pancreas is the major mechanistic pathway that STZ employs to induce hyperglycemia in animals [74,78]. As shown in this study, a similar redox impairment was observed in the pancreatic antioxidant system, with consequent lipid peroxidation in the SO group (Fig. 3D & E). Similar to the differential pattern of antihyperlipidemic effect observed across the three models of interventions, glibenclamide, fermented and unfermented *M. paradisiaca* methanolic extracts showed divergent patterns of antioxidant potential in the pancreas of the STZ-induced diabetes rats. However, fermented *M. paradisiaca* fruit pulp extract showed the most notable impact on MDA level suppression. The consequence of STZ-induced oxidative stress-mediated pancreatic tissue damage has been shown to activate key inflammatory pathways, including N*F*-κB signalling, and upregulate proinflammatory cytokines such as IL-1β, IL-6, and TN*F*-α, thereby exacerbating pancreatic β-cell dysfunction and promoting chronic inflammation in diabetic patients [79–82]. This might account for the elevated proinflammatory markers observed in the STZ-induced diabetes rats group (SO) in this study. The counter-oxidative stress effect of the interventions (SD, SU and SF groups) might have directly or indirectly suppressed some of the proinflammatory markers recorded. However, *f*-PUME intervention inhibits all the makers lower, and comparable to the CG level, thereby suggesting a higher pancreatic protection against STZ-induced inflammation. The reasons may be ascribed to the possible synergistic effect of multiple unique compounds that were identified in our earlier study on fermented *M. paradisiaca* pulp [22].

As discussed earlier in this study, the metabolic derangements induced by STZ, including weight loss, sustained hyperglycemia, impaired glucose tolerance, and dyslipidemia (Figs. 1 and 2), are consequent of widespread systemic stress. This stress cascaded into distorted organosomatic indices of the brain and jejunum (Fig. 4A), diminished protein concentrations in the plasma and tissues (Fig. 4B). This redox homeostasis disruption further escalates into excessive nitric oxide, MDA accumulation (Fig. 4C & E) and GSH depletion (Fig. 4D). These collectively reflect severe oxidative and nutritional imbalance across central and peripheral organs. The elevated organosomatic condition noted in the brain may be ascribed to the disproportional loss of body-to-brain ratio. This finding aligns with the observation of Wang et al. [83], who showed that forebrain volume was unaltered despite the significant body weight loss in the STZ-diabetes Alzheimer's Disease rats' model.

Meanwhile, the proportional jejunal weight loss recorded in this work corroborates the report of Esteves-Monteiro et al. [84]. Kusunoki et al. [85] revealed that there is a positive correlation between the small intestine and body weight loss in diabetic rats is caused by the abnormal increase in acyl-coenzyme A: cholesterol acyltransferase (ACAT) activity in the gastric tract. Both fermented and unfermented *M. paradisiaca* fruit pulp extracts markedly reversed the condition, probably by modulating energy metabolism and protein loss, as both treatments suppressed STZ-induced weight loss, as shown earlier in this study. Fermented *M. paradisiaca* fruit pulp extract showed another and, perhaps, a complementary modulatory dimension in the jejunum by elevating the organosomatic index even beyond that of the SO. This outcome may not be unassociated with the remarkably higher jejunal protein level than its unfermented counterpart and the antidiabetic drug (Fig. 4B). Additionally, L-leucine, a component of leucyl-glycyl-glycine, which was identified in fermented *M. paradisiaca* fruit pulp extract, has been documented to directly [86] and indirectly stimulate intestinal protein synthesis in diverse pathological, nutritional and metabolic states in animal models [87–89].

As revealed in this study, the unfermented, fermented *M. paradisiaca* frui pulp extract and glibenclamide showed antioxidant potential against STZ-induced redox imbalance in non-enzymatic antioxidant (GSH and NO) and lipid peroxidation biomarkers in the plasma, brain and jejunum. Although both unfermented and fermented *M. paradisiaca* fruit pulp extract reversed the STZ-induced oxidative stress, fermented *M. paradisiaca* fruit pulp extract had the highest extent of lipid peroxidation suppression across the three tissues investigated, which was comparable to that of the CG across the three tissues. Bioactive compounds such as gallic acid have been identified in both unripe and fermented *M. paradisiaca* samples [22,90], and have been reported to inhibit oxidative stress in the brain and plasma of STZ-diabetic rats [91, 92]. This might account for the remarkable NO and MDA inhibition, thereby modulating the antioxidants of SF in the plasma, brain, and jejunum of STZ-induced diabetes rats.

Furthermore, the STZ-induced overwhelming systemic and tissue redox imbalance, marked by GSH depletion and surges in NO and MDA, precipitates impairment of the enzymatic antioxidant machinery in the diabetes group (SO). These result in pronounced declines in catalase (CAT), glutathione-S-transferase (GST), and superoxide dismutase (SOD) activities across plasma, brain, and jejunum (Fig. 5). Clearly, the MDA data showed that both unfermented and fermented *M. paradisiaca* fruit pulp extracts reversed the STZ-induced redox imbalance. Both unfermented and fermented *M. paradisiaca* fruit pulp extracts upregulated CAT and SOD activities in all the tissues.

STZ-induced diabetes triggered significant impairments in cholinergic neurotransmission and electrochemical gradients in the brain regions [93,94], and brain membrane-bound enzymes, notably suppressing acetylcholinesterase and Na^+/K^+-ATPase (Table 1). The marked decline in both enzyme activities reflects oxidative stress-induced structural damage to membrane-bound proteins, including oxidation of critical thiol groups and lipid peroxidation within neuronal membranes [16,95]. A resultant disruption of brain membrane redox balance has been linked to compromised membrane integrity, regulation of glucose sensing, neuropeptide signalling, and systemic energy balance [96]. The unfermented *M. paradisiaca* pulp extract shows a mild elevation in both AChE and Na^+/K^+-ATPase above control values, suggesting not only reversal of oxidative inhibition but also possible stimulation of enzyme activities. This stimulation may be attributed to the presence of some antioxidant and neuroactive phytochemicals such as gallic acid, ferulic acid and epicatechin, which are abundantly present in unfermented *M. paradisiaca* pulp, as reported by Rizvi & Zaid [97]. These constituents stimulate erythrocyte membrane-bound AChE and Na^+/K^+-ATPase activities in diabetic conditions, in an insulin-like manner. Also, Kade et al. [98] showed that gallic acid stimulates both AChE and Na^+/K^+-ATPase activities in the brain of diabetic rats. This observation may account for the normalisation of these membrane-bound enzyme activities in the brain, perhaps, by extension, in the hypothalamus. The synergistic effects of these phytochemicals may account for the reestablishment of the brain neurochemical balance, thereby supporting its central role in glycemic regulation. The effect of the fermented *M. paradisiaca* fruit pulp extract on the SF group, on the other hand, seems to produce a more tempered modulation of these enzymes, by elevating AChE activity and partially reversing STZ-induced ATPase suppression. This profile suggests a more distinct neuroprotective effect, possibly due to fermentation-enhanced bioavailability and metabolic conversion of phytochemicals, in addition to the phytochemicals present in its unfermented counterpart. Atunnise et al. [22] identified unique compounds in the fermented *M. paradisiaca* fruit pulp methanolic extract. Some of the compounds

have been reported to have neuroactive and membrane-bound enzyme-stimulating or inhibiting properties. For example, salidroside and coriolic acid's neuroprotective effects have been documented against middle cerebral artery occlusion-induced cerebral stroke via the dopaminergic system [99,100], and spinal cord atrophic condition via gut-microfloral and lipid metabolism [101]. Also, coriolic acid and phytosphingosine, short-chain fatty acids (SCFAs) [22,23,100,102], have been identified in the fermented *M. paradisiaca* fruit extracts, thereby reinforcing the neuronal membrane stability and appetite suppression [103]. While the majority of the reported compounds have been reported to stimulate AChE and Na^+/K^+-ATPase activities, ricinoleic acid may have shown a counter effect because it is a well-established Na^+/K^+-ATPase antagonist. This might have accounted for why fermented *M. paradisiaca* fruit pulp methanolic extract showed a lesser extent of stimulation, comparable to its unfermented counterpart. Hence, establishing that the fermented extract mechanism of action is unique and divergent from its unfermented counterpart.

The histological evidence, including marked shrinkage and morphological distortion of islets, which is evident in the SO group, in this work (Fig. 6), aligns with the well-documented impact of STZ in H&E-stained pancreatic sections of STZ-induced diabetic rats [104]. These observed morphological alterations may be ascribed to the multiple disruptions of biomarkers highlighted in this work. Also, there is an inverse relationship between tissue cytokine levels, especially TN*F*-α, IL-1β and IL-6, and tissue loss. According to an *in-vitro* study by Sonmez Kaplan et al. [105], the elevation of the trio (TNF-α, IL-1β and IL-6) in dental pulp stem cells inhibits their differentiation. The semi-quantitative evaluation in this study further revealed the constituents of the aggregate outcome in the histological image. The pronounced islet enlargement and hypercellularity seen in the unfermented *M. paradisiaca* fruit pulp extract-treated group may be partly ascribed to the direct proportionality of brain AChE activity observed in this work. Paes et al. [106] reported that elevated AChE in the autonomic nervous system stimulates pancreatic AChE expression. This is a phenomenon that favours pancreatic endocrine cell hyperplasia in persistent hyperinsulinemic hypoglycemia conditions [107] and probable tumorgenesis [108]. In a twist, fermented *M. paradisiaca* fruit pulp extract may have addressed this probable complication by modestly stimulating the AChE activity. Hence, accounting for the near-normal histomorphogenic outcome seen in this work.

Aldehyde-fuchsin selectively highlights β-cell granules. The resultant disruption in insulin secretion by STZ administration is obvious in the SO group, and this is consistent with the histological evidence that has been reported [109]. As observed in this study, the graded improvement in GAF reactivity with the unfermented and especially the fermented *M. paradisiaca* fruit pulp methanolic extracts (SU, SF) may be attributed to some of the phytoconstituents [22,110]. The improved islet-dimension, area, border integrity, elevated β-cell density and insulin production, and non-endocrine area reduction, as observed in this current work, could be attributed to the enhanced antioxidant enzyme activities, suppression of proinflammatory agents and both endo- and exogenous glycemic regulations of pancreatic tissue.

In STZ-induced diabetes, the neuroenteric integrity and architecture are profoundly disrupted. The hypothalamus, a central regulatory hub for energy balance and glycemic homeostasis, exhibits marked vulnerability to oxidative injury [111]. All these are evident by the decreased neuronal nuclei density and increased cytoplasmic vacuolation in the hypothalamic regions of the SO group (Fig. 8). These pathological changes mirror systemic and cerebral oxidative injury, which compromise neuroendocrine signalling, a process critical for insulin sensitivity, glucose sensing, and metabolic regulation [112]. Both histological and morphometric evidence in this study (Figs. 8 and 9) aligned with these neurodegenerative alterations. However, the unfermented and fermented *M. paradisiaca* fruit pulp methanolic extracts employed in this study reversed the majority of these pathological changes. Also, our interventions increased hypothalamic nuclear density while decreasing vacuole counts, an indication of enhanced neuronal proliferation and mitigation of STZ-induced oxidative damage.

The bidirectional relationship between the jejunum and other energy-metabolism regulatory sites like the pancreas and hypothalamus has made the jejunum one of the focal points [113,114] in diabetic conditions. Hence, jejunal functional and structural integrity becomes a pivotal factor in diabetes induction and progression [115,116]. This may account for jejunal morphological disruption and architectural integrity compromise observed in this study (SO). Despite STZ exclusively targeting the pancreas, the jejunum is significantly injured in the diabetes groups as histomorphometric evidence revealed profound mucosal and crypt disruption, characterised by crypt hyperplasia, vacuolation, and lamina propria inflammation. This condition further reinforces hyperglycemia and impairs central-peripheral metabolic coordination. Hence, showing an interplay between jejunal structure, pancreatic endocrine function, and hypothalamic metabolic regulation under STZ-induced diabetic conditions [115]. The moderate improvement in jejunal morphology seen in SU indicates that unfermented *M paradisiaca* fruit pulp extract partially mitigates diabetes-associated stress at the jejunal level, as reflected by improved villus definition but incomplete restoration of crypt–villus organisation and other morphometric indices in this work. The near-control jejunal architecture, with elongated villi and distinctive crypt structure seen in the SF, may be ascribed directly or indirectly to the component in the fermented extract. For example, methyl-gallate has been reported to promote intestinal villi growth and integrity by inhibiting the TLR_4/NFκB pathway in ulcerative colitis conditions [117].

5. Conclusion

This finding demonstrates that the methanolic extract of fermented *M. paradisiaca* fruit pulp methanolic extract exerts a broad and antidiabetic action in STZ-induced diabetes in male rats. The fermented extract uniquely restored body-weight trajectories and fasting glycemia to near-control levels, outperforming its unfermented counterpart and a known antidiabetic drug. Also, it ameliorated dyslipidemia by modestly suppressing total cholesterol, triglycerides, LDL-c, and non-HDL-c fraction while stabilising HDL-c, thereby reducing atherogenic and coronary heart disease risk indices. The oral administration of this extract for 42 days preserved pancreatic, brain and jejunal integrity by normalising organosomatic indices, protein content, insulin secretion, and antioxidant system and suppresses lipid peroxidation. In addition, it markedly increased pancreatic insulin secretion, inhibited pro-inflammatory cytokines, and culminated in improved islet morphometric indices and β-cell granule density. Furthermore, fermented *M. paradisiaca* fruit pulp methanolic extract modulates the histoarchitecture of both hypothalamus and jejunum by reversing STZ-induced neuronal vacuolation, pyknotic nuclei, crypt hyperplasia, and inflammatory infiltrates. This study has shown that fermented M. paradisiaca fruit pulp methanolic extract exhibits a marked anti-hyperglycemic effect via antioxidant activity, normalisation of glucose and lipid metabolism, organoprotection, and restoration of enteroneuronal morphological and functional integrity, hence may serve as a multitargeted alternative for diabetes management. Future studies should focus on detailed pharmacokinetics, dose-response optimisation, mechanistic dissection in other models, and potential translation into clinical interventions.

Funding

The authors received no external funding for the work. The authors provided funding.

Declaration of Competing Interest

The authors declare no competing interests.

Acknowledgements

The authors are grateful to the Departments of Biochemistry and Industrial Chemistry, Redeemer's University, and the Directorate of the Centre for Chemical and Biochemical Research, Redeemer's University, for providing laboratory facilities and equipment towards the success of this study.

References

[1] American Diabetes Association, Diagnosis and classification of diabetes mellitus, Diabetes Care 37 (2014) S81–S90, https://doi.org/10.2337/dc14-S081.
[2] International Diabetes Federation, IDF Diabetes Atlas 2025, 11th ed., International Diabetes Federation, 2025. https://diabetesatlas.org/ (accessed December 30, 2025).
[3] T. Tönnies, W. Rathmann, A. Hoyer, R. Brinks, O. Kuss, Quantifying the underestimation of projected global diabetes prevalence by the International Diabetes Federation (IDF) Diabetes Atlas, BMJ Open. Diabetes Res. Care 9 (2021) e002122, https://doi.org/10.1136/bmjdrc-2021-002122.
[4] E. Papachristoforou, V. Lambadiari, E. Maratou, K. Makrilakis, Association of glycemic indices (hyperglycemia, glucose variability, and hypoglycemia) with oxidative stress and diabetic complications, J. Diabetes Res. 2020 (2020) 7489795, https://doi.org/10.1155/2020/7489795.
[5] J.S. Bhatti, A. Sehrawat, J. Mishra, I.S. Sidhu, U. Navik, N. Khullar, S. Kumar, G. K. Bhatti, P.H. Reddy, Oxidative stress in the pathophysiology of type 2 diabetes and related complications: current therapeutics strategies and future perspectives, Free. Radic. Biol. Med. 184 (2022) 114–134, https://doi.org/10.1016/J.FREERADBIOMED.2022.03.019.
[6] P. Richards, N.A. Thornberry, S. Pinto, The gut–brain axis: Identifying new therapeutic approaches for type 2 diabetes, obesity, and related disorders, Mol. Metab. 46 (2021) 101175, https://doi.org/10.1016/j.molmet.2021.101175.
[7] P. Meerarani, J. Badimon, E. Zias, V. Fuster, P. Moreno, Metabolic syndrome and diabetic atherothrombosis: implications in vascular complications, Curr. Mol. Med. 6 (2006) 501–514, https://doi.org/10.2174/156652406778018680.
[8] L. Luciani, M. Pedrelli, P. Parini, Modification of lipoprotein metabolism and function driving atherogenesis in diabetes, Atherosclerosis 394 (2024) 117545, https://doi.org/10.1016/J.ATHEROSCLEROSIS.2024.117545.
[9] H.F. Azhari, J. Dawson, The impacts of new antidiabetic drugs on the risk of ischemic and hemorrhagic strokes: a comprehensive review and meta-analysis of clinical trials, Front. Stroke 3 (2024), https://doi.org/10.3389/fstro.2024.1363954.
[10] V. Prentza, G. Pavlidis, I. Ikonomidis, S. Pililis, S. Lampsas, A. Kountouri, L. Pliouta, E. Korakas, J. Thymis, L. Palaiodimou, A. Tsegka, K. Markakis, P. Halvatsiotis, G. Tsivgoulis, V. Lambadiari, Antidiabetic treatment and prevention of ischemic stroke: a systematic review, J. Clin. Med. 13 (2024), https://doi.org/10.3390/jcm13195786.
[11] N. Kurita, K. Yamashiro, T. Kuroki, R. Tanaka, T. Urabe, Y. Ueno, N. Miyamoto, M. Takanashi, H. Shimura, T. Inaba, Y. Yamashiro, K. Nomoto, S. Matsumoto, T. Takahashi, H. Tsuji, T. Asahara, N. Hattori, Metabolic endotoxemia promotes neuroinflammation after focal cerebral ischemia, J. Cereb. Blood Flow. Metab. 40 (2020) 2505–2520, https://doi.org/10.1177/0271678X19899577;WEBSITE:WEBSITE:SAGE;WGROUP:STRING:PUBLICATION.
[12] C.A. Thaiss, M. Levy, I. Grosheva, D. Zheng, E. Soffer, E. Blacher, S. Braverman, A. C. Tengeler, O. Barak, M. Elazar, R. Ben-Zeev, D. Lehavi-Regev, M.N. Katz, M. Pevsner-Fischer, A. Gertler, Z. Halpern, A. Harmelin, S. Aamar, P. Serradas, A. Grosfeld, H. Shapiro, B. Geiger, E. Elinav, Hyperglycemia drives intestinal barrier dysfunction and risk for enteric infection, Science 359 (2018) 1376–1383, https://doi.org/10.1126/SCIENCE.AAR3318.
[13] M. Zhao, J. Chu, S. Feng, C. Guo, B. Xue, K. He, L. Li, Immunological mechanisms of inflammatory diseases caused by gut microbiota dysbiosis: a review, Biomed. & Pharmacother. 164 (2023) 114985, https://doi.org/10.1016/j.biopha.2023.114985.
[14] P.D. Cani, M. Van Hul, C. Lefort, C. Depommier, M. Rastelli, A. Everard, Microbial regulation of organismal energy homeostasis, Nat. Metab. 1 (2019) 34–46, https://doi.org/10.1038/S42255-018-0017-4.
[15] S. Rai, S. Sreelatha, N. Devang, P.D. Alva, A.V. Raveendran, The microbiota–gut–brain axis and diabetic cognitive impairment: a memorable journey, Clin. Diabetol. 12 (2023) 261–271, https://doi.org/10.5603/DK.a2023.0025.
[16] O.L. Adebayo, G.E. Luro, I.D. Akeju, C.F. Onu, M.E. Fawehinmi, V.A. Aderemi, A. K. Atunnise, Sodium butyrate ameliorates mitochondrial oxidative stress and alterations in membrane-bound enzyme activities in pentylenetetrazole-induced kindling rat model, Metab. Brain Dis. 40 (2025), https://doi.org/10.1007/S11011-025-01550-9.
[17] O.L. ADEBAYO, V.A. AGU, G.A. IDOWU, B.C. EZEJIAKU, A.K. ATUNNISE, The role of vitamin C on ATPases activities in monosodium glutamate-induced oxidative stress in rat striatum and cerebellum, Neurotox. Res. 42 (2024), https://doi.org/10.1007/S12640-024-00719-X.
[18] S. Yagihashi, H. Mizukami, K. Sugimoto, Mechanism of diabetic neuropathy: where are we now and where to go? J. Diabetes Investig. 2 (2011) 18–32, https://doi.org/10.1111/j.2040-1124.2010.00070.x.
[19] A. Verrotti, G. Prezioso, R. Scattoni, F. Chiarelli, Autonomic neuropathy in diabetes mellitus, Front. Endocrinol. (Lausanne). 5 (2014), https://doi.org/10.3389/fendo.2014.00205.
[20] S. Padhi, A.K. Nayak, A. Behera, Type II diabetes mellitus: a review on recent drug based therapeutics, Biomed. & Pharmacother. 131 (2020) 110708, https://doi.org/10.1016/j.biopha.2020.110708.
[21] N.M. Mindrescu, C. Guja, V. Jinga, S. Ispas, A. Curici, A. Nelson Twakor, A. M. Pantea Stoian, Interactions between gut microbiota and oral antihyperglycemic drugs: a systematic review, Int. J. Mol. Sci. 25 (2024) 3540, https://doi.org/10.3390/ijms25063540.
[22] A.K. Atunnise, O. Bodede, A. Adewuyi, V. Maharaj, G. Prinsloo, B.A. Salau, Metabolomics and in-vitro bioactivities studies of fermented Musa paradisiaca pulp: a potential alpha-amylase inhibitor, Heliyon 10 (2024) e24659, https://doi.org/10.1016/j.heliyon.2024.e24659.
[23] A. Adeleke, S. Tioluwani, O. Kuburat Te, O. David Olum, A. Moronke Mu, S. Bamidele A, Enhancement of bioactive compounds during fermentation of unripe Musa paradisiaca, Trends Appl. Sci. Res. 15 (2020) 115–124, https://doi.org/10.3923/tasr.2020.115.124.
[24] M.F. Afzal, W. Khalid, S. Akram, M.A. Khalid, M. Zubair, S. Kauser, K. Abdelsamea Mohamedahmed, A. Aziz, S. Anusha Siddiqui, Bioactive profile and functional food applications of banana in food sectors and health: a review, Int. J. Food Prop. 25 (2022) 2286–2300, https://doi.org/10.1080/10942912.2022.2130940.
[25] O.E. Similoluwa, O.A. Okhonlaye, A.A. Openla, A.I. Moses, A.-M.O. Benjamin, G. P. Oladimeji, A.J. Olaseni, Antinutrient contents of fermented and extruded unripe plantain and Pigeon Pea blends, South. Asian J. Res. Microbiol. (2022) 17–24, https://doi.org/10.9734/SAJRM/2022/V14I1260.
[26] E.A. Ugbogu, V.C. Ude, I. Elekwa, U.O. Arunsi, C. Uche-Ikonne, C. Nwakanma, Toxicological profile of the aqueous-fermented extract of Musa paradisiaca in rats, Avicenna J. Phytomed. 8 (2018) 478–487.
[27] K.A. Ajijolakewu, A.S. Ayoola, T.O. Agbabiaka, F.R. Zakariyah, N.R. Ahmed, O. J. Oyedele, A. Sani, A review of the ethnomedicinal, antimicrobial, and phytochemical properties of Musa paradisiaca (plantain), Bull. Natl. Res. Cent. 45 (2021) 86, https://doi.org/10.1186/s42269-021-00549-3.
[28] I.O. Bolanle, E.K.I. Omogbai, E.E. Bafor, Effects of amlodipine and valsartan on glibenclamide-treated streptozotocin-induced diabetic rats, Biomed. & Pharmacother. 106 (2018) 566–574, https://doi.org/10.1016/j.biopha.2018.06.152.
[29] A.I. Olagunju, T.D. Oluwajuyitan, S.I. Oyeleye, Effect of plantain bulb's extract-beverage blend on blood glucose levels, antioxidant status, and carbohydrate hydrolysing enzymes in streptozotocin-induced diabetic rats, Prev. Nutr. Food Sci. 25 (2020) 362, https://doi.org/10.3746/PNF.2020.25.4.362.
[30] A. Ghasemi, S. Jeddi, Streptozotocin as a tool for induction of rat models of diabetes: a practical guide, EXCLI J. 22 (2023) 274, https://doi.org/10.17179/excli2022-5720.
[31] B.L. Furman, Streptozotocin-induced diabetic models in mice and rats, Curr. Protoc. 1 (2021) e78, https://doi.org/10.1002/CPZ1.78.
[32] U. Galicia-Garcia, A. Benito-Vicente, S. Jebari, A. Larrea-Sebal, H. Siddiqi, K. B. Uribe, H. Ostolaza, C. Martín, Pathophysiology of type 2 diabetes mellitus, 2020, Vol. 21, Page 6275, Int. J. Mol. Sci. 21 (2020) 6275, https://doi.org/10.3390/IJMS21176275.
[33] T. Baylie, A. Kebad, T. Ayelgn, M. Tiruneh, K. Hunie Tesfa, Anti-Diabetic Effects of the 80% Methanolic Extract of Datura stramonium Linn (Solanaceae) Leaves in Streptozotocin- Induced Diabetic Mice, J. Exp. Pharmacol. 15 (2023) 375–389, https://doi.org/10.2147/JEP.S426925.
[34] B. Legeza, P. Marcolongo, A. Gamberucci, V. Varga, G. Bánhegyi, A. Benedetti, A. Odermatt, Fructose, glucocorticoids and adipose tissue: implications for the metabolic syndrome, Nutrients (2017), https://doi.org/10.3390/nu9050426.
[35] O.H. LOWRY, N.J. ROSEBROUGH, A.L. FARR, R.J. RANDALL, Protein measurement with the Folin phenol reagent, J. Biol. Chem. 193 (1951) 265–275. http://www.ncbi.nlm.nih.gov/pubmed/14907713.
[36] W.T. Friedewald, R.I. Levy, D.S. Fredrickson, Estimation of the concentration of low-density lipoprotein cholesterol in plasma, without use of the preparative ultracentrifuge, Clin. Chem. 18 (1972) 499–502.
[37] W.P. Castelli, R.D. Abbott, P.M. McNamara, Summary estimates of cholesterol used to predict coronary heart disease, Circulation 67 (1983) 730–734, https://doi.org/10.1161/01.CIR.67.4.730.
[38] R.D. Abbott, P.W. Wilson, W.B. Kannel, W.P. Castelli, High density lipoprotein cholesterol, total cholesterol screening, and myocardial infarction. The Framingham Study, Arterioscler. Off. J. Am. Heart Assoc. Inc. 8 (1988) 207–211, https://doi.org/10.1161/01.ATV.8.3.207.
[39] M. Dobiášová, J. Frohlich, The plasma parameter log (TG/HDL-C) as an atherogenic index: Correlation with lipoprotein particle size and esterification rate inapob-lipoprotein-depleted plasma (FERHDL), Clin. Biochem. 34 (2001) 583–588, https://doi.org/10.1016/S0009-9120(01)00263-6.
[40] J.I. Cleeman, Executive Summary of The Third Report of The National Cholesterol Education Program (NCEP) Expert Panel on Detection, Evaluation, And Treatment of High Blood Cholesterol In Adults (Adult Treatment Panel III), JAMA 285 (2001) 2486–2497, https://doi.org/10.1001/JAMA.285.19.2486.
[41] E. Beutler, B.M. Kelly, The effect of sodium nitrite on red cell GSH, Experientia 19 (1963) 96–97, https://doi.org/10.1007/BF02148042.
[42] N.S. Bryan, M.B. Grisham, Methods to detect nitric oxide and its metabolites in biological samples, Free. Radic. Biol. Med. 43 (2007) 645–657, https://doi.org/10.1016/j.freeradbiomed.2007.04.026.

[43] R. Varshney, R.K. Kale, Effects of Calmodulin Antagonists on Radiation-induced Lipid Peroxidation in Microsomes, Int. J. Radiat. Biol. 58 (1990) 733–743, https://doi.org/10.1080/09553009014552121.
[44] H. Luck, Methods of Enzymatic analysis, 2, Academia Press, New York, 1974, pp. 885–894.
[45] K. Nadarajapillai, D.S. Liyanage, S. Sellaththurai, T. Jeong, S. Lee, J. Lee, Glutathione-S-transferase alpha-4 in Hippocampus abdominalis (big-belly seahorse): Molecular characterization, antioxidant properties, and its potent immune response, Comparative Biochemistry Physiology Part - C Toxicology Pharmacology 240 (2021), https://doi.org/10.1016/J.CBPC.2020.108917.
[46] H.P. Misra, I. Fridovich, The Role of Superoxide Anion in the Autoxidation of Epinephrine and a Simple Assay for Superoxide Dismutase, J. Biol. Chem. 247 (1972), https://doi.org/10.1016/S0021-9258(19)45228-9.
[47] G.L. Ellman, K.D. Courtney, V. Andres, R.M. Featherstone, A new and rapid colorimetric determination of acetylcholinesterase activity, Biochem. Pharmacol. 7 (1961) 88–95, https://doi.org/10.1016/0006-2952(61)90145-9.
[48] J.P. Quigley, G.S. Gotterer, Distribution of (Na+-K+-stimulated ATPase activity in rat intestinal mucosa, Biochim. Et. Biophys. Acta (BBA) - Biomembr. 173 (1969) 456–468, https://doi.org/10.1016/0005-2736(69)90010-8.
[49] D.J. Stewart, Sensitive automated methods for phosphate and (Na+ + K+)-ATPase, Anal. Biochem. 62 (1974) 349–364, https://doi.org/10.1016/0003-2697(74)90167-5.
[50] J.A. Ramos-Vara, Technical aspects of immunohistochemistry, Vet. Pathol. 42 (2005) 405–426, https://doi.org/10.1354/VP.42-4-405.
[51] J.D. Bancroft, M. Gamble, Theory and Practice of Histological Techniques, Sixth Edition, Theory and Practice of Histological Techniques, Sixth Ed. (2007) 1–725, https://doi.org/10.1097/NEN.0B013E31817E2933.
[52] C.A. Schneider, W.S. Rasband, K.W. Eliceiri, NIH Image to ImageJ: 25 years of image analysis, Nat. Methods 9 (2012) 671–675, https://doi.org/10.1038/NMETH.2089;SUBJMETA=1647,245,631,794;KWRD=IMAGING,SOFTWARE.
[53] T.A. da Silva, R.M. Lemes, C.J.F. Oliveira, A. da S. Almeida, J.E.L. Chica, Data on morphometric analysis of the pancreatic islets from C57BL/6 and BALB/c mice, Data Brief. 8 (2016) 1094–1098, https://doi.org/10.1016/j.dib.2016.07.030.
[54] G. Kilimnik, J. Jo, V. Periwal, M.C. Zielinski, M. Hara, Quantification of islet size and architecture, Islets 4 (2012) 167–172, https://doi.org/10.4161/isl.19256.
[55] A.R. Diani, G.A. Sawada, B.A. Hannah, K.S. Jodelis, M.A. Connell, C.L. Connell, T. J. Vidmar, B.M. Wyse, Analysis of pancreatic islet cells and hormone content in the spontaneously diabetic KKAy mouse by morphometry, immunocytochemistry and radioimmunoassay, Virchows Arch. A Pathol. Anat. Histopathol. 412 (1987) 53–61, https://doi.org/10.1007/BF00750731.
[56] A.C. Ruifrok, D.A. Johnston, Quantification of histochemical staining by color deconvolution, Anal. Quant. Cytol. Histol. 23 (2001) 291–299.
[57] Z. Bibi, D.A. Bukhari, M.Q. Sarwar, S. Arifullah, T. Younas, A. Manzoor, Rehman, Gut health improvement by locally isolated probiotics and histomorphometric analysis in Wistar rats, Curr. Res. Biotechnol. 9 (2025) 100271, https://doi.org/10.1016/j.crbiot.2024.100271.
[58] R. Lakshman, M. Najami, J.M. Allen, J. Ware, M.E. Wilinska, S. Hartnell, A. Thankamony, T. Randell, A. Ghatak, R.E.J. Besser, D. Elleri, N. Trevelyan, F. M. Campbell, R. Hovorka, C.K. Boughton, Diabetic ketoacidosis at onset of type 1 diabetes and glycemic outcomes with closed-loop insulin delivery, Diabetes Technol. Ther. 26 (2024) 198–202, https://doi.org/10.1089/DIA.2023.0307.
[59] M.Jodeiri Farshbaf, T.A. Matos, K. Niblo, Y. Alokam, J.L. Ables, STZ-induced hyperglycemia differentially influences mitochondrial distribution and morphology in the habenulointerpeduncular circuit, Front. Cell. Neurosci. 18 (2024) 1432887, https://doi.org/10.3389/FNCEL.2024.1432887/FULL.
[60] O. Anachad, A. Taouil, W. Taha, F. Bennis, F. Chegdani, The implication of short-chain fatty acids in obesity and diabetes, 117863612311627, Microbiol. Insights 16 (2023), https://doi.org/10.1177/11786361231162720.
[61] L. Wen, F.S. Wong, Dietary short-chain fatty acids protect against type 1 diabetes, Nat. Immunol. 18 (2017) 484–486, https://doi.org/10.1038/NI.3730.
[62] O.M. Agunloye, Y.F. Ogunyanmodi, K.M. Adebanjo, G. Oboh, Blood glucose and blood pressure lowering effect of diets supplemented with whole unripe plantain flour and effects on altered biomolecules in diabetic/hypertensive rats, Discov. Food 4 (2024), https://doi.org/10.1007/S44187-024-00229-X.
[63] O. Adekunle, Ajiboye, A. Sidiqat, Diet supplemented with boiled unripe plantain (Musa paradisiaca) exhibited antidiabetic potentials in streptozotocin-induced Wistar rats, J. Food Biochem. 46 (2022) e14431, https://doi.org/10.1111/JFBC.144314.
[64] A. Gastaldelli, Abdominal fat: does it predict the development of type 2 diabetes? Am. J. Clin. Nutr. 87 (2008) 1118–1119, https://doi.org/10.1093/ajcn/87.5.1118.
[65] B.E. Corkey, Diabetes: Have We Got It All Wrong? Diabetes Care 35 (2012) 2432–2437, https://doi.org/10.2337/dc12-0825.
[66] B.B. Dokken, The Pathophysiology of Cardiovascular Disease and Diabetes: Beyond Blood Pressure and Lipids, Diabetes Spectr. 21 (2008) 160–165, https://doi.org/10.2337/diaspect.21.3.160.
[67] D.J. Magliano, R.M. Islam, E.L.M. Barr, E.W. Gregg, M.E. Pavkov, J.L. Harding, M. Tabesh, D.N. Koye, J.E. Shaw, Trends in incidence of total or type 2 diabetes: systematic review, BMJ (2019) l5003, https://doi.org/10.1136/bmj.l5003.
[68] D. Rokicka, B. Hudzik, M. Wróbel, T. Stołtny, D. Stołtny, A. Nowowiejska-Wiewióra, S. Rokicka, M. Gąsior, K. Strojek, Prognostic value of novel atherogenic indices in patients with acute myocardial infarction with and without type 2 diabetes, J. Diabetes Complicat. 38 (2024) 108850, https://doi.org/10.1016/j.jdiacomp.2024.108850.
[69] C.M. Ballantyne, T.C. Andrews, J.A. Hsia, J.H. Kramer, C. Shear, Correlation of non-high-density lipoprotein cholesterol with apolipoprotein B: Effect of 5 hydroxymethylglutaryl coenzyme A reductase inhibitors on non-high-density lipoprotein cholesterol levels, Am. J. Cardiol. 88 (2001) 265–269, https://doi.org/10.1016/S0002-9149(01)01638-1.
[70] J. Cai, S. Lu, Z. Yao, Y.P. Deng, L.Di Zhang, J.W. Yu, G.F. Ren, F.M. Shen, G. J. Jiang, Glibenclamide attenuates myocardial injury by lipopolysaccharides in streptozotocin-induced diabetic mice, Cardiovasc. Diabetol. 13 (2014), https://doi.org/10.1186/S12933-014-0106-Y.
[71] S. Lenzen, Oxidative stress: the vulnerable β-cell, Biochem. Soc. Trans. 36 (2008) 343–347, https://doi.org/10.1042/BST0360343.
[72] M.Y. Donath, S.E. Shoelson, Type 2 diabetes as an inflammatory disease, Nat. Rev. Immunol. 11 (2011) 98–107, https://doi.org/10.1038/NRI2925.
[73] J.W. Baynes, S.R. Thorpe, Role of oxidative stress in diabetic complications: a new perspective on an old paradigm, Diabetes 48 (1999) 1–9, https://doi.org/10.2337/diabetes.48.1.1.
[74] A.A. Like, A.A. Rossini, Streptozotocin-induced pancreatic insulitis: new model of diabetes mellitus, Science (1979) 193 (1976) 415–417, https://doi.org/10.1126/SCIENCE.180605.
[75] K. Srinivasan, B. Viswanad, L. Asrat, C.L. Kaul, P. Ramarao, Combination of high-fat diet-fed and low-dose streptozotocin-treated rat: a model for type 2 diabetes and pharmacological screening, Pharmacol. Res. 52 (2005) 313–320, https://doi.org/10.1016/J.PHRS.2005.05.004.
[76] E.F. Lhoste, I. Catala, M. Fiszlewicz, A.M. Gueugneau, F. Popot, P. Vaissade, T. Corring, O. Szylit, Influence of caecal microflora and of two dietary protein levels on the adaptation of the exocrine pancreas: comparative study in germ-free and conventional rats, Br. J. Nutr. 75 (1996) 433–444, https://doi.org/10.1079/BJN19960145.
[77] A.O. Iyoriobhe, A.O. Abiola, P.A. Adedigba, P.H. Fagbenro, T.A. Adebisi, F. A. Idowu, A.S. Ogunbowale, O.A. Abisogun, S.A. Adeniyi, O.B. Adu, B.O. Elemo, Protein isolates from fermented melon seeds promoted differential expression in liver and pancreas of streptozotocin induced diabetic male wistar rats, Asian J. Biochem. Genet. Mol. Biol. (2020) 6–18, https://doi.org/10.9734/AJBGMB/2020/V5I330130.
[78] P.L. Cruz, I.C. Moraes-Silva, A.A. Ribeiro, J.F. Machi, M.D.T. de Melo, F. dos Santos, M.B. da Silva, C.M.C. Strunz, E.G. Caldini, M.C. Irigoyen, Nicotinamide attenuates streptozotocin-induced diabetes complications and increases survival rate in rats: role of autonomic nervous system, BMC Endocr. Disord. 21 (2021), https://doi.org/10.1186/S12902-021-00795-6.
[79] D.L. Eizirik, M.L. Colli, F. Ortis, The role of inflammation in insulitis and β-cell loss in type 1 diabetes, Nat. Rev. Endocrinol. 5 (2009) 219–226, https://doi.org/10.1038/nrendo.2009.21.
[80] M.Y. Donath, S.E. Shoelson, Type 2 diabetes as an inflammatory disease, Nat. Rev. Immunol. 11 (2011) 98–107, https://doi.org/10.1038/nri2925.
[81] J.L. Evans, I.D. Goldfine, B.A. Maddux, G.M. Grodsky, Oxidative Stress and Stress-Activated Signaling Pathways: A Unifying Hypothesis of Type 2 Diabetes, Endocr. Rev. 23 (2002) 599–622, https://doi.org/10.1210/er.2001-0039.
[82] S. Lenzen, The mechanisms of alloxan- and streptozotocin-induced diabetes, Diabetologia 51 (2008) 216–226, https://doi.org/10.1007/s00125-007-0886-7.
[83] J.Q. Wang, J. Yin, Y.F. Song, L. Zhang, Y.X. Ren, D.G. Wang, L.P. Gao, Y.H. Jing, Brain Aging and AD-Like Pathology in Streptozotocin-Induced Diabetic Rats, J. Diabetes Res. 2014 (2014) 796840, https://doi.org/10.1155/2014/796840.
[84] M. Esteves-Monteiro, D. Menezes-Pinto, M. Ferreira-Duarte, P. Dias-Pereira, M. Morato, M. Duarte-Araújo, Histomorphometry Changes and Decreased Reactivity to Angiotensin II in the Ileum and Colon of Streptozotocin-Induced Diabetic Rats, Int. J. Mol. Sci. 23 (2022) 13233, https://doi.org/10.3390/IJMS232113233/S1.
[85] J. Kusunoki, K. Aragane, T. Kitamine, H. Kozono, K. Kano, K. Fujinami, K. Kojima, T. Chiwata, Y. Sekine, Postprandial hyperlipidemia in streptozotocin-induced diabetic rats is due to abnormal increase in intestinal acyl coenzyme A:cholesterol acyltransferase activity, Arterioscler. Thromb. Vasc. Biol. 20 (2000) 171–178, https://doi.org/10.1161/01.ATV.20.1.171/ASSET/A2D5CCCC-96F6-4C64-902E-3C0D0107CDBE/ASSETS/GRAPHIC/HQ0201144005.JPEG.
[86] D.H. Alpers, Protein Synthesis in Intestinal Mucosa: the Effect of Route of Administration of Precursor Amino Acids, J. Clin. Invest. 51 (1972) 167–173, https://doi.org/10.1172/JCI106788.
[87] Y. Chang, H. Cai, G. Liu, W. Chang, A. Zheng, S. Zhang, R. Liao, W. Liu, Y. Li, J. Tian, Effects of dietary leucine supplementation on the gene expression of mammalian target of rapamycin signaling pathway and intestinal development of broilers, Anim. Nutr. 1 (2015) 313, https://doi.org/10.1016/J.ANINU.2015.11.005.
[88] X. Mao, M. Liu, J. Tang, H. Chen, D. Chen, B. Yu, J. He, J. Yu, P. Zheng, Dietary Leucine Supplementation Improves the Mucin Production in the Jejunal Mucosa of the Weaned Pigs Challenged by Porcine Rotavirus, PLoS. One 10 (2015) e0137380, https://doi.org/10.1371/JOURNAL.PONE.0137380.
[89] J.S. Hirschfield, F. Kern, Protein starvation and the small intestine: III. Incorporation of orally and intraperitoneally administered l-leucine 4,5–3 H into intestinal mucosal protein of protein-deprived rats, J. Clin. Investig. 48 (1969) 1224, https://doi.org/10.1172/JCI106086.
[90] S. Ola Salawu, Antioxidant Activities, Nutrient Composition and Sensory Properties of Unripe Plantain-Purple Skinned Sweet Potato Flour Blends, Journal of Natural Sciences Research Www.Iiste.Org ISSN 5 (2015). www.iiste.org (accessed June 21, 2025).
[91] F. Ramezani Ali Akbari, M. Badavi, M. Dianat, S.A. Mard, A. Ahangarpour, GALLIC ACID IMPROVES OXIDATIVE STRESS AND INFLAMMATION THROUGH REGULATING MICRORNAS EXPRESSIONS IN THE BLOOD OF DIABETIC RATS, Acta Endocrinol. (Buchar.) 15 (2019) 187, https://doi.org/10.4183/AEB.2019.187.

[92] P.S. Mainzen Prince, M.R. Kumar, C.J. Selvakumari, Effects of gallic acid on brain lipid peroxide and lipid metabolism in streptozotocin-induced diabetic Wistar rats, J. Biochem. Mol. Toxicol. 25 (2011) 101–107, https://doi.org/10.1002/jbt.20365.
[93] S. Antony, P. Kumar T, J. Mathew, T.R. Anju, C.S. Paulose, Hypoglycemia induced changes in cholinergic receptor expression in the cerebellum of diabetic rats, 2010 17:1, J. Biomed. Sci. 17 (2010) 7, https://doi.org/10.1186/1423-0127-17-7.
[94] B. Welsh, L. Wecker, Effects of streptozotocin-induced diabetes on acetylcholine metabolism in rat brain, Neurochem. Res. 16 (1991) 453–460, https://doi.org/10.1007/BF00965566.
[95] E.O. Olufunmilayo, M.B. Gerke-Duncan, R.M.D. Holsinger, Oxidative Stress and Antioxidants in Neurodegenerative Disorders, 2023, Vol. 12, Page 517, Antioxidants 12 (2023) 517, https://doi.org/10.3390/ANTIOX12020517.
[96] T. Gong, D.J. Torres, M.J. Berry, M.W. Pitts, Hypothalamic redox balance and leptin signaling - Emerging role of selenoproteins, Free. Radic. Biol. Med. 127 (2018) 172, https://doi.org/10.1016/j.freeradbiomed.2018.02.038.
[97] S.I. Rizvi, M.A. Zaid, Insulin-Like Effect Of (–)Epicatechin On Erythrocyte Membrane Acetylcholinesterase Activity In Type 2 Diabetes Mellitus, Clin. Exp. Pharmacol. Physiol. 28 (2001) 776–778, https://doi.org/10.1046/j.1440-1681.2001.03513.x.
[98] I.J. Kade, J.B.T. Rocha, Gallic acid modulates cerebral oxidative stress conditions and activities of enzyme-dependent signaling systems in streptozotocin-treated rats, Neurochem. Res. 38 (2013) 761–771, https://doi.org/10.1007/S11064-013-0975-6.
[99] Z.F. Zhong, J. Han, J.Z. Zhang, Q. Xiao, J.Y. Chen, K. Zhang, J. Hu, L.D. Chen, Neuroprotective effects of salidroside on cerebral ischemia/reperfusion-induced behavioral impairment involves the dopaminergic system, Front. Pharmacol. 10 (2019) 483469, https://doi.org/10.3389/FPHAR.2019.01433/BIBTEX.
[100] L. Zhang, S. Sui, S. Wang, J. Sun, Neuroprotective Effect of Corosolic Acid Against Cerebral Ischemia-Reperfusion Injury in Experimental Rats, J. Oleo Sci. 71 (2022) 1501–1510, https://doi.org/10.5650/JOS.ESS22130.
[101] Y. Feng, Y. Cui, J. Jin, S. Huang, J. Wei, M. Yao, D. Zhou, S. Mao, The alterations of gut microbiome and lipid metabolism in patients with spinal muscular atrophy, Neurol. Ther. 12 (2023) 961–976, https://doi.org/10.1007/s40120-023-00477-6.
[102] Y.M. Bashmil, F.R. Dunshea, R. Appels, H.A.R. Suleria, Bioaccessibility of phenolic compounds, resistant starch, and dietary fibers from australian green banana during in vitro digestion and colonic fermentation, Molecules 29 (2024) 1535, https://doi.org/10.3390/MOLECULES29071535.
[103] G. Frost, M.L. Sleeth, M. Sahuri-Arisoylu, B. Lizarbe, S. Cerdan, L. Brody, J. Anastasovska, S. Ghourab, M. Hankir, S. Zhang, D. Carling, J.R. Swann, G. Gibson, A. Viardot, D. Morrison, E.L. Thomas, J.D. Bell, The short-chain fatty acid acetate reduces appetite via a central homeostatic mechanism, Nat. Commun. 5 (2014) 3611, https://doi.org/10.1038/NCOMMS4611.
[104] T. Szkudelski, The mechanism of alloxan and streptozotocin action in B cells of the rat pancreas, Physiol. Res. 50 (2001) 537–546.
[105] S. Sonmez Kaplan, H. Sazak Ovecoglu, D. Genc, T. Akkoc, TNF-α, IL-1B and IL-6 affect the differentiation ability of dental pulp stem cells, BMC Oral. Health 23 (2023) 1–10, https://doi.org/10.1186/S12903-023-03288-1/FIGURES/6.
[106] A.M.A. PAES, S.R. CARNIATTO, F.A. FRANCISCO, N.A. BRITO, P.C.F. MATHIAS, ACETYLCHOLINESTERASE ACTIVITY CHANGES ON VISCERAL ORGANS OF VMH LESION–INDUCED OBESE RATS, Int. J. Neurosci. 116 (2006) 1295–1302, https://doi.org/10.1080/00207450600920910.
[107] D. Ouyang, D. Dhall, R. Yu, Pathologic pancreatic endocrine cell hyperplasia, World J. Gastroenterol. 17 (2011) 137–143, https://doi.org/10.3748/wjg.v17.i2.137.
[108] B. Pérez-Aguilar, J.U. Marquardt, E. Muñoz-Delgado, R.M. López-Durán, M. C. Gutiérrez-Ruiz, L.E. Gomez-Quiroz, J.L. Gómez-Olivares, Changes in the Acetylcholinesterase Enzymatic Activity in Tumor Development and Progression, Cancers (Basel) 15 (2023), https://doi.org/10.3390/cancers15184629.
[109] Yang, Intraperitoneal co-administration of thymosin α-1 ameliorates streptozotocin-induced pancreatic lesions and diabetes in C57BL/6 mice, Int. J. Mol. Med. 23 (2009), https://doi.org/10.3892/ijmm_00000169.
[110] S. Sundaram Chinna Krishnan, I. Pillai Subramanian, S. Pillai Subramanian, Isolation, characterization of syringin, phenylpropanoid glycoside from Musa paradisiaca tepal extract and evaluation of its antidiabetic effect in streptozotocin-induced diabetic rats, Biomed. & Prev. Nutr. 4 (2014) 105–111, https://doi.org/10.1016/j.bionut.2013.12.009.
[111] A. Drougard, A. Fournel, P. Valet, C. Knauf, Impact of hypothalamic reactive oxygen species in the regulation of energy metabolism and food intake, Front. Neurosci. 9 (2015) 105341, https://doi.org/10.3389/fnins.2015.00056.
[112] C. Zhang, X. Zhang*, Regulation of Glucose Homeostasis by Hypothalamic Nuclei, Pract. Med. Res. 2 (2024), https://doi.org/10.18686/pmr.v2i2.4439.
[113] B. Lkhagvasuren, O. Mee-inta, Z.W. Zhao, T. Hiramoto, D. Boldbaatar, Y.M. Kuo, Pancreas-Brain Crosstalk, Front. Neuroanat. 15 (2021) 691777, https://doi.org/10.3389/fnana.2021.691777.
[114] D.L. Sigalet, O. Bawazir, G.R. Martin, L.E. Wallace, G. Zaharko, A. Miller, A. Zubaidi, Glucagon-like peptide-2 induces a specific pattern of adaptation in remnant jejunum, Dig. Dis. Sci. 51 (2006) 1557–1566, https://doi.org/10.1007/s10620-006-9077-5.
[115] L. Castagneto-Gissey, G. Angelini, J.R. Casella-Mariolo, P. Marini, G. Mingrone, G. Casella, The jejunum is the key factor in insulin resistance, Surg. Obes. Relat. Dis. 16 (2020) 509–519, https://doi.org/10.1016/j.soard.2019.12.024.
[116] C. Osinski, L. Le Gléau, C. Poitou, J. de Toro-Martin, L. Genser, M. Fradet, H. A. Soula, A. Leturque, C. Blugeon, L. Jourdren, E.L. Hubert, K. Clément, P. Serradas, A. Ribeiro, Type 2 diabetes is associated with impaired jejunal enteroendocrine GLP-1 cell lineage in human obesity, Int. J. Obes. (Lond.) 45 (2021) 170–183, https://doi.org/10.1038/s41366-020-00694-1.
[117] P. Zhou, J. Lai, Y. Li, J. Deng, C. Zhao, Q. Huang, F. Yang, S. Yang, Y. Wu, X. Tang, F. Huang, L. Wang, X. Huang, W. Zou, J. Wu, Methyl gallate alleviates acute ulcerative colitis by modulating gut microbiota and inhibiting TLR4/NF-κB pathway, Int. J. Mol. Sci. 23 (2022) 14024, https://doi.org/10.3390/ijms232214024.